NASA CR-120966
AVSD-0336-72-CR

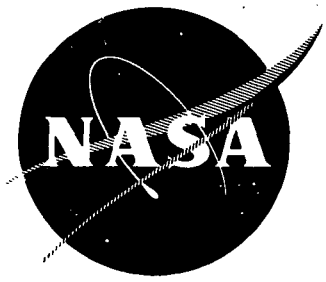

HIGH TEMPERATURE COMPOUNDS FOR TURBINE VANES

by W.H. Rhodes and R.M. Cannon, Jr.

AVCO SYSTEMS DIVISION
Lowell, Massachusetts

Prepared for

NATIONAL AERONAUTICS AND SPACE ADMINISTRATION

NASA Lewis Research Center
Contract NAS3-14333
William A. Sanders, Project Manager

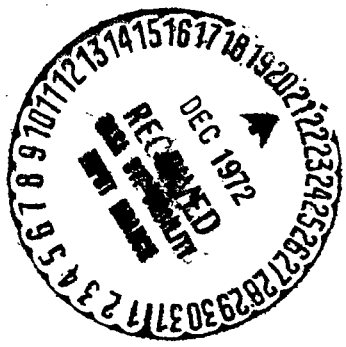

1. Report No.	2. Government Accession No.	3. Recipient's Catalog No.
NASA-CR 120966		

4. Title and Subtitle	5. Report Date
High Temperature Compounds for Turbine Vanes (U)	September 1972
	6. Performing Organization Code

7. Author(s)	8. Performing Organization Report No.
W.H. Rhodes R.M. Cannon, Jr.	
	10. Work Unit No.

9. Performing Organization Name and Address	11. Contract or Grant No.
Avco Corporation Systems Division Lowell, Mass. 01851	NAS3-14333
	13. Type of Report and Period Covered
12. Sponsoring Agency Name and Address	Contractor Report
National Aeronautics & Space Administration Washington, D.C. 20546	14. Sponsoring Agency Code

15. Supplementary Notes

Project Manager, William A. Sanders
NASA Lewis Research Center, Cleveland, Ohio

16. Abstract

Fabrication and microstructure control studies were conducted on SiC, Si_3N_4, and composites based on these compounds. Charpy mode impact testing to 2400°F established that β-spodumene, lithium aluminum silicate, coated Si_3N_4, Si_3N_4 derived from α-Si_3N_4 powder, and SiC containing 5-25 v/o chopped C fibers had the most promising strengths. Several other composite systems had excellent microstructures and could prove interesting materials in the future. Stress-rupture testing on Si_3N_4 established that increasing 2000°F - 100 hour strengths were obtained for increasing grain size to at least 5 μm, increasing density and possibly increasing phase purity. These parameters became less important at 2400°F where it is thought a grain boundary phase controls strength.

17. Key Words (Suggested by Author(s))	18. Distribution Statement
Composites Turbine Materials Ceramics Mechanical Properties of Ceramics Silicon Carbide Silicon Nitride	Unclassified - Unlimited

19. Security Classif. (of this report)	20. Security Classif. (of this page)	21. No. of Pages	22. Price*
Unclassified	Unclassified	69	$3.00

* For sale by the National Technical Information Service, Springfield, Virginia 22151

FOREWORD

The research described herein was conducted by the Avco Corporation, Systems Division, under NASA Contract NAS3-14333. The work was done under the management of the NASA Project Manager, Mr. William A. Sanders, Materials and Structures Division, NASA Lewis Research Center. Dr. William H. Rhodes was the Principal Investigator with Mr. Rowland M. Cannon, Jr. assisting in materials evaluation. Other Avco personnel who contributed significantly to this project were Philip Foley, Ernest Vallante, John Centorino, Burton MacAllister, Charles Houck, Philip Berneburg, Russell Gardner, and John Zgrebnak.

Page Intentionally Left Blank

TABLE OF CONTENTS

Page

LIST OF FIGURES

LIST OF TABLES

I. SUMMARY

The objective of this program was to determine the feasibility of improving the mechanical behavior of high temperature composites to such a degree that they may become candidate materials for use as turbine stator vanes in advanced turbine engines. The compounds studied were SiC and Si_3N_4 alone and with powders, fibers, or whisker additions to make composites. Primary emphasis was given toward improving the mechanical impact resistance at temperatures between 2000°F - 2400°F. The influence of Si_3N_4 microstructures and process variables on stress rupture life were also studied. Material development was conducted with a goal of retaining the demonstrated oxidation resistance and thermal shock stability of the matrix.

Composite compositions were from 5 to 65 volume percent additive phase. Whisker additions were SiC and Si_3N_4. Carbon and various oxidation resistant metals were added as chopped fibers or wires. Considerable attention was given to Si_3N_4 powders and the consolidated phases and microstructure. Consolidation was accomplished by the hot pressing method. Selected composites were either given polishing treatments or β-spodumene, lithium aluminum silicate coatings in an attempt to remove surface flaws or introduce compressive surface layers.

Si_3N_4 fabricated from α-Si_3N_4 powder had impact strengths up to a factor of 4 higher than Si_3N_4 made with α-Si_3N_4 powder or compared with SiC billets. The Si_3N_4 impact strength was further improved by a factor of 2 for some of the specimens coated with β-spodumene. Polished Si_3N_4 specimens exhibited impact strength improvements of from 5-30 percent depending on test temperature. The impact strength of SiC was improved by up to a factor of 2.5 for 5-25 volume percent addition of chopped carbon fibers. The systems Si_3N_4/SiC whiskers, Si_3N_4 wire, Si_3N_4/Mo wire, and Si_3N_4/Si_3N_4 whiskers had promising microstructures which suggested that with optimization one or more of these systems could exhibit improved impact strengths.

The 2000°F (1366°K) stress rupture strength for Si_3N_4 was found to increase with increasing grain size from 1 μm to 5 μm, and increasing density. A possible strength relation with phase purity was discovered. Unexpectedly, MgO densification aid concentrations between 1-4 wt. % gave equivalent strengths. Limited 2400°F (1589°K) testing demonstrated nearly equivalent stress-rupture strengths for the various Si_3N_4 billets suggesting that the plasticity of a grain boundary phase such as $MgSiO_3$ controls strength at that temperature.

Page Intentionally Left Blank

II. INTRODUCTION

Higher gas turbine inlet temperatures will improve engine efficiency which means specific fuel and air consumption will decrease with power per unit weight increasing. These incentives as well as reduced gas pollution problems lend considerable inducement toward developing materials that can perform efficiently in a higher temperature turbine environment both in the vane and blade configuration. Materials for the vane application with its lower mechanical stress requirements are expected to be available first. Preliminary testing at a number of facilities indicate that SiC and Si_3N_4 base materials have the necessary oxidation resistance, thermal shock resistance, strength, stress rupture life and chemical stability for consideration. An initial program conducted at Avco(ref. 1) found that Si_3N_4 appears to be superior in thermal shock resistance and strength, whereas SiC has better oxidation resistance and stress rupture life. It was also found that SiC whisker additions raised the impact strength of the matrix materials which was low and was expected to be a very real limiting property for turbine applications of interest to NASA. The impact resistance is necessary in order for a ceramic part to withstand impact by a foreign body without catastrophic failure to it or to other parts of the engine. Therefore, a major objective of this program was to raise the mechanical shock resistance of these materials.

The problem of impact resistance of brittle ceramics is complex and as yet not fully understood. However, the desired impact resistance can be viewed in terms of two somewhat different requirements:

1) The body should be able to withstand an impact without being damaged, i.e. without crack initiation or growth of pre-existent flaws.

2) The body should dissipate sufficient energy that, if a crack is started, it may be stopped without catastrophic failure.

Except for loading modes with strongly inhomogeneous stress fields, the second criteria will be difficult to satisfy for most ceramic materials; however, even if the piece fails, it is desirable to reduce the size and kinetic energy of the fragments.

For brittle materials the strength is determined by the condition for crack propagation which is essentially given by the effective surface energy for fracture, γ_f, and the stress concentration resulting from pre-existing flaws. The relation between these is given by some modification of the Griffith condition(ref. 2) such as:

$$\sigma = \sqrt{\frac{2E\gamma_f}{\pi c}} \qquad (1)$$

where c is the half length of the critical flaw, E the elastic modulus and σ the fracture strength; the exact shape of the flaw will result in small differences in the numerical constants as a result of the stress concentration.(ref. 3)

For either of the impact resistance considerations, increasing the fracture surface energy, γ_f, will increase the impact resistance. However, material modifications which increase γ_f may also increase the average flaw size, reducing static strength. Therefore, the design of composites for impact will depend on the relative importance placed on the two different impact criteria and should depend on the magnitude and mode of mechanical impact which is anticipated in service. For a gas turbine application, it may be reasonable to assume that the prolonged exposure effects of thermal fatigue, creep and oxidation may increase c during service so that the greater emphasis should be placed on maximizing γ_f. The use of a destructive impact energy criterion (such as the Charpy type of test) will have the effect of biasing the results in this direction, although the results with unnotched bars indicate that the test is sensitive both to increases in γ_f and to reduction in flaw size as reflected in static strength.

For the present program, material alterations, or composite designs, which would provide an increase in γ_f were emphasized, although an effort was also made to achieve good static strength in most cases. The fracture surface energy can be viewed as having several additive components:

$$\gamma_f = \gamma_o + W_p + G_c \qquad (2)$$

The first term, γ_o, is the free energy of the two new surfaces created; W_p is the energy consumed by plastic deformation and G_c includes a number of different crack propagation effects. For the various ceramics which could be considered, significant changes in γ_o cannot be obtained to provide the large increases in γ_f necessary.

In ductile systems, the plastic work term, W_p, is several orders of magnitude higher than either of the other two terms.(ref. 4) However, for the ceramic systems considered, significant contributions from plastic work cannot be expected even at the service temperatures of interest. Even though some creep deformation may occur, the yield mechanisms are so strain rate sensitive that very little, if any, plastic deformation can occur under impact conditions. As a result, the only way a significant plastic contribution can be obtained is through the use of a more ductile second phase. The additions of a metallic second phase would be expected to provide an increase in the fracture energy by plastic deformation in the vicinity of the propagating crack. The effect on γ_f will depend strongly on the morphology of the metallic phase, since the crack must be forced to propagate through the ductile phase for it to be effective. As a result, continuous networks or filamentary distributions would be more effective for impact resistance, although they may be more detrimental to creep resistance and oxidation resistance.

The last term in equation (2), G_c, which is herein termed the irreversible work of brittle fracture, includes several energy consuming processes associated with propagation of the crack and its interaction with the microstructure. It is this area in which microstructural variations such as porosity and grain size and morphology can significantly increase the fracture surface energy in ceramics. Whenever the crack deviates from an essentially flat surface to form steps, jogs or branches, there is an increase in γ_f. These increases are, in part, a result of the increase in real area over the

nominal area of the crack front; however, the increase in γ_f is generally greater than can be attributed simply to this area increase(ref 5) so that this effect is also included in G_c. Increases in fracture energy have been predicted to result from the interaction of discreet particles with the crack front.(ref. 6) With the use of fibrous or whisker additions, even stronger effects may be expected. If the whiskers or fibers are sufficiently strong, passage of the main crack will require additional cracking along the fiber-matrix interface and this can significantly increase the propagation energy.

With these criteria, composites based on SiC and Si_3N_4 with reinforcement elements consisting of whisker or fiber additions in the 5-65 v/o range were fabricated and tested. The whiskers considered were SiC and Si_3N_4; while carbon was added as a filamentary addition. Also, metal additions in the 2-10 v/o were added to Si_3N_4. Efforts were also devoted toward upgrading the basic matrix properties, particularly for Si_3N_4.

III. COMPOSITE FABRICATION

A. General

One serious problem in the fabrication of composites is uniform mixing of the whiskers or fibers. Recent work(ref. 7) to fabricate diboride/carbon composites demonstrated that uniform composites could be formed by first preparing a well-dispersed high solid content slip, then casting, drying, and shaping to conform to the hot pressing die. All fiber or whisker additive systems for this program were prepared by first dispersing the matrix powder in a glyceral media followed by hand stirring the additive into a 1000 centipoise slip. The final slip was given a 15 sec. final mix in a Waring blender prior to casting into a $1\frac{1}{2}$-inch diameter plaster mold. After drying to the stiff plastic stage, the disc was forged to $2\frac{1}{2}$ inches in diameter to affect fiber alignment.

Final consolidation was achieved by hot pressing in a $2\frac{1}{2}$-inch inside diameter graphite die. A graphite insulation system was employed which resulted in a predominant CO pressing atmosphere. Partial pressures of CO_2, N, and Ar were also present due to the equilibrium balance with CO, entrapped air, and seepage from the flushed sight tube, respectively.

In the following sections the fabrication and characterization of the base matrix compositions and composites will be discussed treating each material system separately.

B. Silicon Carbide Base Systems

1. Silicon Carbide

a. Powder

The three SiC powder sources listed in Table I were considered as matrix powders. Table I includes supplier generated powder characteristics

as well as data generated in this program and indicates that the Carborundum SiC was the purest.

TABLE I. - CHARACTERISTICS OF SILICON CARBIDE POWDERS

Supplier	Phase Analysis	Impurities	Particle Size
Carborundum	α SiC	0.02 Si 0.86 SiO_2	4 μm
Elek. (Wacker)	-	< 0.2% Si	4 μm
Dow Corning	β SiC	10% C 1% Halogen	0.01 μm

Figure 1 illustrates the crystallite size and morphology for the Carborundum and Elektroschemlzwerk powder. Both powders showed little evidence for agglomeration and had very angular crystallites. Both characteristics are common for powders reduced to their ultimate size by grinding. The particle size noted in these electron shadowgraphs was within the range measurable by the Coulter Counter and the particle size distributions are shown in Figure 2. There appears to be little advantage of one powder over another based strictly on powder morphology.

An electron photomicrograph of the Dow Corning SiC was supplied with the powder and exhibited a fine cubic morphology. It was thought that this small particle size would be a great asset in reduction of the hot pressing temperature as predicted by the Herring(ref. 8) Scaling Law for a diffusional densification process. The high impurity level was expected to be troublesome, however. This powder was purified for one run by heating in air at 1112°F (873°K) for 1 hour to remove C followed by washing with HF to remove SiO_2 and washing with HNO_3 to remove Si.

b. Consolidation

Unreinforced SiC using the Carborundum powder was not pressed during this period as the previous program(ref. 1) has taught that > 98% density and an 8-20 μm grain size could be achieved. The consolidation experiments listed in Table II were conducted with the Elektroschemlzwerk and Dow Corning powder. A density of 97.6% was achieved for pressing D1549 with the Elek. powder under conditions previously found acceptable for Carborundum powder. A microstructural examination revealed the occurrence of exaggerated grain growth in the 50-500 μm range and a small amount of porosity entrapped with the grains. Pressings D1591A and D1591B were conducted under a reduced thermal cycle to reduce grain size. The grain size was reduced to 45 μm, but with a penalty of 1.3% loss of density. Electron microscopic examination and the prismatic grain morphology of sample 1549 suggest the presence of a thin grain boundary phase.

Four consolidation experiments were conducted with the Dow Corning powder. These pressings were conducted at temperatures far lower than normally employed for SiC under the hypothesis that the finer crystallite

70006 (a) 1500X

71178 (b) 1500X

Figure 1. Electron Shadowgraph of SiC Powder From (a) Carborundum and (b) Elektroschemlzwerk.

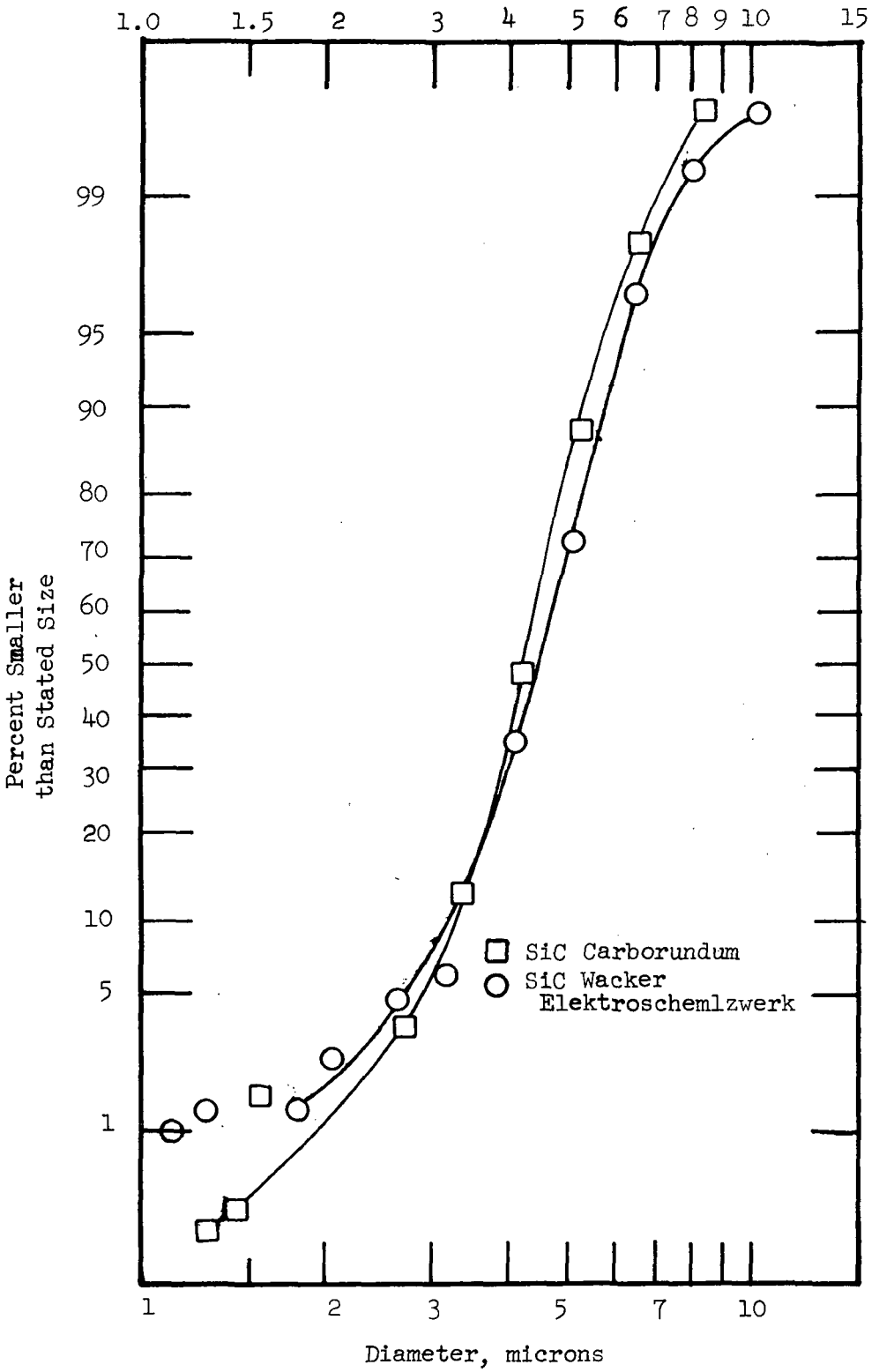

Figure 2. Crystallite Size Distribution for SiC Powders.

TABLE II

FABRICATION CONDITIONS FOR SiC

Run No.	Material	Additive	Temp. °F	Temp. °K	Pressure Psi	Pressure MN/m^2	Time min.	Density gm/cc	Density $Kg/m^3 \times 10^3$
D1549	Elek. SiC	3 w/o Al_2O_3	4064	2513	4000	27.5	250	3.13	3.13
D1591A	Elek. SiC	3 w/o Al_2O_3	3884	2413	4000	27.5	240	3.09	3.09
D1591B	Elek. SiC	3 w/o Al_2O_3, 1 w/o C	3884	2413	4000	27.5	240	3.01	3.01
1607	Dow C SiC	None	2804	1833	5000	34.5	35	1.15	1.15
1611	Dow SiC	None	3272	2073	5000	34.5	64	1.77	1.77
R1611	Dow SiC	None	3632	2273	5000	34.5	60	1.80	1.80
1612	Dow SiC	None, but purified	3488	2193	5000	34.5	62	1.50	1.50

size should permit reduced pressing temperature, allowing the use of reinforcements that normally react with SiC during the higher temperature consolidation cycle. Another departure from usual practice was the deliberate omission of the Al_2O_3 densification aid. Little densification occurred at pressing temperatures from 2804°F to 3632°F. The latter temperature was only 250°F lower than that required to produce 97% dense SiC using Carborundum powder plus Al_2O_3 densification aid. Purified powder was used for the last pressing, 1612, and it appears that purification reduces the reactivity of the powder. Based on the fact that this powder did not provide the desired reduction in pressing temperature, this powder was eliminated from further consideration.

These experiments with Dow Corning's 100 Å powder contrasted with previous work on Carborundum's 40,000 Å powder, strongly suggests that the normal diffusive densification model does not apply to SiC. The Herring(ref. 8) Scaling Law, together with the appropriate densification model, would predict a 10^8 increase in densification rate for the fine powder. This conclusion is supported by the fact that a densification aid was required to hot press dense SiC. It has been suggested that densification occurs via a liquid phase mechanism.(ref. 9) Even the liquid phase sintering models predict that densification rate is $\propto r^{-1}$. However, verification experiments using a densification aid and the fine SiC powder were not conducted.

The Elektroschemlzwerk powder was judged moderately acceptable, but due to the difficulty in obtaining a 10-20 μm grain size, together with high density, it was decided to use Carborundum SiC powder as the matrix powder.

2. Silicon Carbide plus Silicon Carbide Whiskers

a. Silicon Carbide Whiskers

Several billets have previously(ref. 1) been hot pressed in this system using 1 μm by 30 μm Carborundum SiC whiskers. It was impossible to conclude by metallographic examination that whiskers were retained. It was reasoned that the whisker morphology was destroyed by grain growth during processing. Since such a reaction was obviously kinetics limited, larger SiC whiskers would be a correct step toward whisker retention. Such whiskers were available from two sources: National Research Division of Cabot and Elektroschemlzwerk. Whiskers from the two sources had an identical morphological appearance as illustrated in Figure 3. The effective size was 3 μm by 50 μm. According to Cabot, their whiskers are α-SiC and were measured to have a 70 x 10^6 psi elastic modulus and an average 300 x 10^3 psi tensile strength.

b. Consolidation

The hot pressing runs for this system are listed in Table III. The experiments are listed with increasing SiC whisker concentrations.

Preforms were prepared by the slip casting-cold flow process described in Section III.A. Pressings D1596 and D1621 resulted in acceptable relative densities of 97.5% and 97.2% for SiC whisker volume loadings of 38% and 50%, respectively. A volume loading of 65% SiC whiskers caused some difficulty as it was necessary to repress the billet with a peak temperature of 4064°F to reach 95.7% relative density which was judged acceptable for mechanical evaluation.

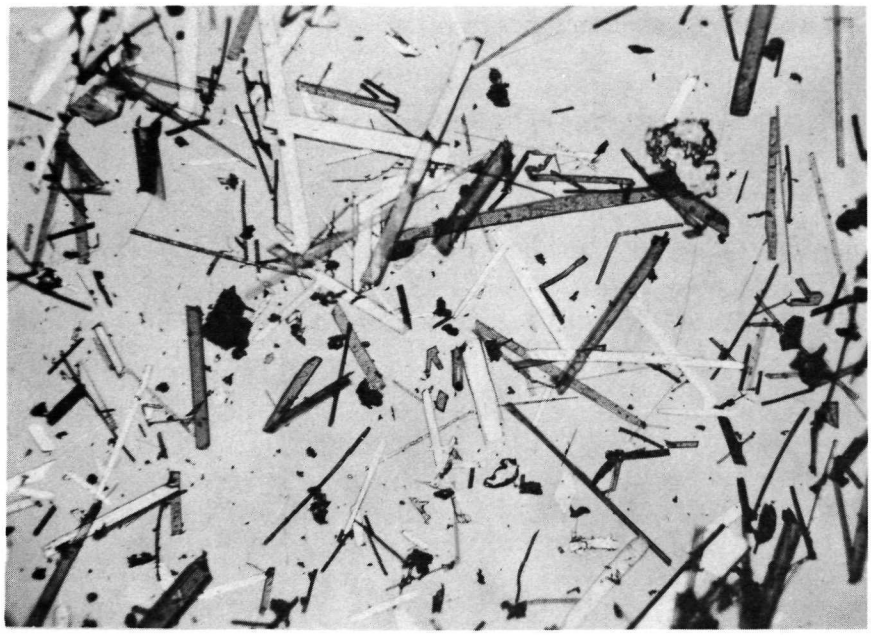

5502-2 50X

Figure 3. SiC Whiskers

Four attempts were made to achieve high density at the 5 and 10 v/o SiC whisker concentration. Again peak temperatures of 4064°F were employed, but only 92.3% density was achieved for the 5% loading and 88.5% for the 10% loading. These were judged unsuitable for mechanical evaluation.

The nature of the SiC hot pressing consolidation mechanism is not well known. However, it is postulated that SiC whiskers could impede densification by particle re-arrangement or grain boundary sliding. Thus, it could be expected that densification would be difficult to achieve with SiC whiskers in a SiC matrix. It is not understood why the intermediate volume loadings densified while concentrations at both the high and low end had slow densification kinetics.

Microstructure

The microstructure of this system is illustrated by sample D1596 which contained 38 v/o SiC whiskers (Figure 4). Particulate carbon (2 w/o) was added to this billet to combine with free Si. Based on the second phase in Figure 4a, it appears that the carbon concentration level was too high and the 150 μm size of several inclusions must detract from strength. The apparent porosity is consistent with the 97.5% density. The pore size was fine, which is thought to be advantageous. The etched structure (Figure 4b) illustrates that the whiskers were retained and aligned preferentially. The long axes were aligned normal to both the cold forging and hot pressing direction. Some whiskers were broken during pressing, but the overall whisker retention was judged excellent. Some matrix/whisker interaction was noted by the ratcheted whisker boundaries. The matrix grain size was 20 μm, which was low due to the whiskers impeding growth. Specimens D1621 and D1673

TABLE III

FABRICATION CONDITIONS FOR THE SiC PLUS SiC WHISKER SYSTEM

Run No.	Material	Additive	Temp. °F	Temp. °K	Pressure Psi	Pressure MN/m^2	Time min.	Density gm/cc	Density $Kg/m^3 \times 10^3$
1756	Carb. SiC	3 w/o Al_2O_3 5 v/o SiC	3938 4064	2443 2513	4000	27.5	120 275	2.95	2.95
1735	Carb. SiC	3 w/o Al_2O_3 10 v/o SiC	3938	2443	4000	27.5	180	2.66	2.66
1738	Carb. SiC	3 w/o Al_2O_3 10 v/o SiC	3938	2443	4000	27.5	180	2.75	2.75
1744	Carb. SiC	3 w/o Al_2O_3 10 v/o SiC	4064	2513	4000	27.5	240	2.83	2.83
D1596*	Carb. SiC	3 w/o Al_2O_3 2 w/o C 38 v/o SiC	3884	2413	4000	27.5	180	3.12	3.12
D1621*	Carb. SiC	3 w/o Al_2O_3 50 v/o SiC	3938	2443	4000	27.5	180	3.11	3.11
1673	Carb. SiC	3 w/o Al_2O_3 65 v/o SiC	3884	2413	4000	27.5	180	2.93	2.93
1673*	Repress SiC	3 w/o Al_2O_3 65 v/o SiC	4064	2513	4000	27.5	180	3.06	3.06

*Impact tested.

5515-2 (a) 100X

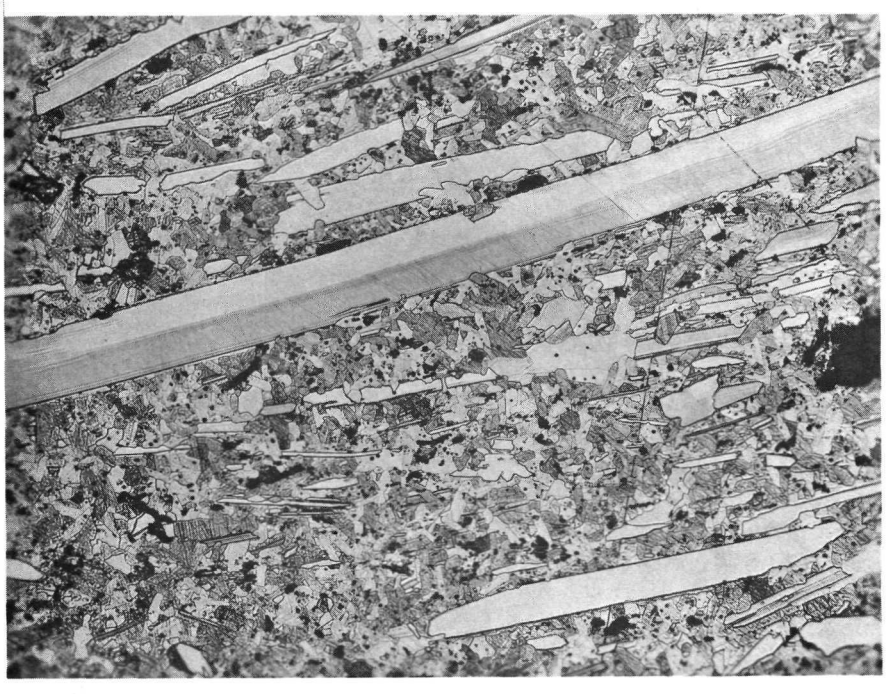

5515-4 (b) 100X

Figure 4. SiC plus 38 v/o SiC Whiskers, D1596, Showing (a) Overall As-polished Microstructure, and (b) Etched Structure Viewing Plane Parallel to the Pressing Direction.

with higher volume loading were not significantly different microstructurally other than the higher whisker contents and absence of free carbon.

3. Silicon Carbide Plus Carbon Fibers

a. Carbon Fibers

The carbon reinforcing filaments considered were Great Lakes carbon monofilament, Fiber Technology's low E (elastic modulus) or medium E filament, Union Carbide's Thornel 50 and Thornel 75 filaments, and Avco's low E filament. In order to realize the maximum potential gain in fracture surface energy and as well as any benefit from the standard composite reinforcement principles, it was decided to use the highest modulus, highest strength filament. Thus, Thornel 75 with an elastic modulus of 79 x 10^6 psi and tensile strength of 380 Kpsi was selected. It was also decided to perform preliminary mixing and fabrication experiments with Avco's low E filament which possessed an elastic modulus of 8 x 10^6 psi and strength of 120 Kpsi. Other than cost, the main justification for using the Avco filament was that the difference in matrix/fiber elastic properties were maximized serving to test the importance of this variable on crack branching which might be quite different for the two moduli fibers.

b. Consolidation

The billets fabricated with this system are listed in Table IV. Billet 1574 was the only billet fabricated using the Avco carbon fibers. The percent relative density calculated from the bulk density depends quite markedly on the density value assigned to the C filament. Prior to hot pressing, the density of Thornel 75 was taken as 1.8 gm/cc. However, during hot pressing, it is possible that the fibers densified to a density value approaching 2.2 gm/cc, that for highly graphitized C. Figure 5 illustrates the theoretical composite density versus composition using the two end values for density of the C phase. Also shown are the bulk densities of the billets selected for mechanical evaluation. All but one of the selected billets fall within the envelope for fully dense material. The low density billet at 50 v/o C (D1679) is between 87.0 - 93.7% dense.

In general, the C fiber composites densified readily. Typically, a temperature of 3884°F for 180 minutes was sufficient, whereas 4064°F for 240 minutes failed to densify some of the billets having SiC whisker additions. It is thought that C either in fiber or particulate is beneficial to the hot pressing kinetics. It is difficult to postulate that the combination of C with free Si would give this result, but perhaps C reduces and reacts with SiO_2. SiO_2, even though it is liquid during hot pressing, could interfere with the normal densification process for SiC.

c. Microstructure

Figure 6 illustrates the as-polished structure for the two orientations relative to the pressing direction. The chopped carbon fibers are strongly aligned normal to the pressing direction. As with previous systems, alignment was achieved by three processes: casting a slip, cold forging a partially dried slip, and hot pressing. The relative contribution of each step to the orientation is unknown. The matrix structure appears quite dense with only a small amount of a finely divided pore phase remaining.

TABLE IV

FABRICATION CONDITIONS FOR THE SiC PLUS C FIBER SYSTEM

Run No.	Material	Additive	Temp. °F	Temp. °K	Pressure Psi	Pressure MN/m^2	Time min.	Density gm/cc	Density $Kg/m^3 \times 10^3$
D1754*	Carb. SiC	3 w/o Al_2O_3 5 v/o C	3938	2443	4000	27.5	180	3.15	3.15
D1745*	Carb. SiC	3 w/o Al_2O_3 10 v/o C	3884	2413	4000	27.5	180	3.09	3.09
D1574*	Carb. SiC	3 w/o Al_2O_3 25 v/o C	3884	2413	3000	20.6	95	2.89	2.89
D1583	Carb. SiC	3 w/o Al_2O_3 25 v/o C	3884	2413	3000	20.6	170	2.82	2.82
D1592	Carb. SiC	3 w/o Al_2O_3 25 v/o C	3884	2413	4000	27.5	180	2.90	2.90
D1594*	Carb. SiC	3 w/o Al_2O_3 25 v/o C	3884	2413	4000	27.5	180	2.96	2.96
D1584	Carb. SiC	3 w/o Al_2O_3 38 v/o C	3884	2413	3000	20.6	176	2.86	2.86
D1615*	Carb. SiC	3 w/o Al_2O_3 38 v/o C	3884	2413	4000	27.5	180	2.71	2.71
D1611	Carb. SiC	3 w/o Al_2O_3 50 v/o C	3884	2413	4000	27.5	180	2.27	2.27
D1679*	Carb. SiC	3 w/o Al_2O_3 50 v/o C	3884	2413	4000	27.5	220	2.35	2.35

*Impact tested.

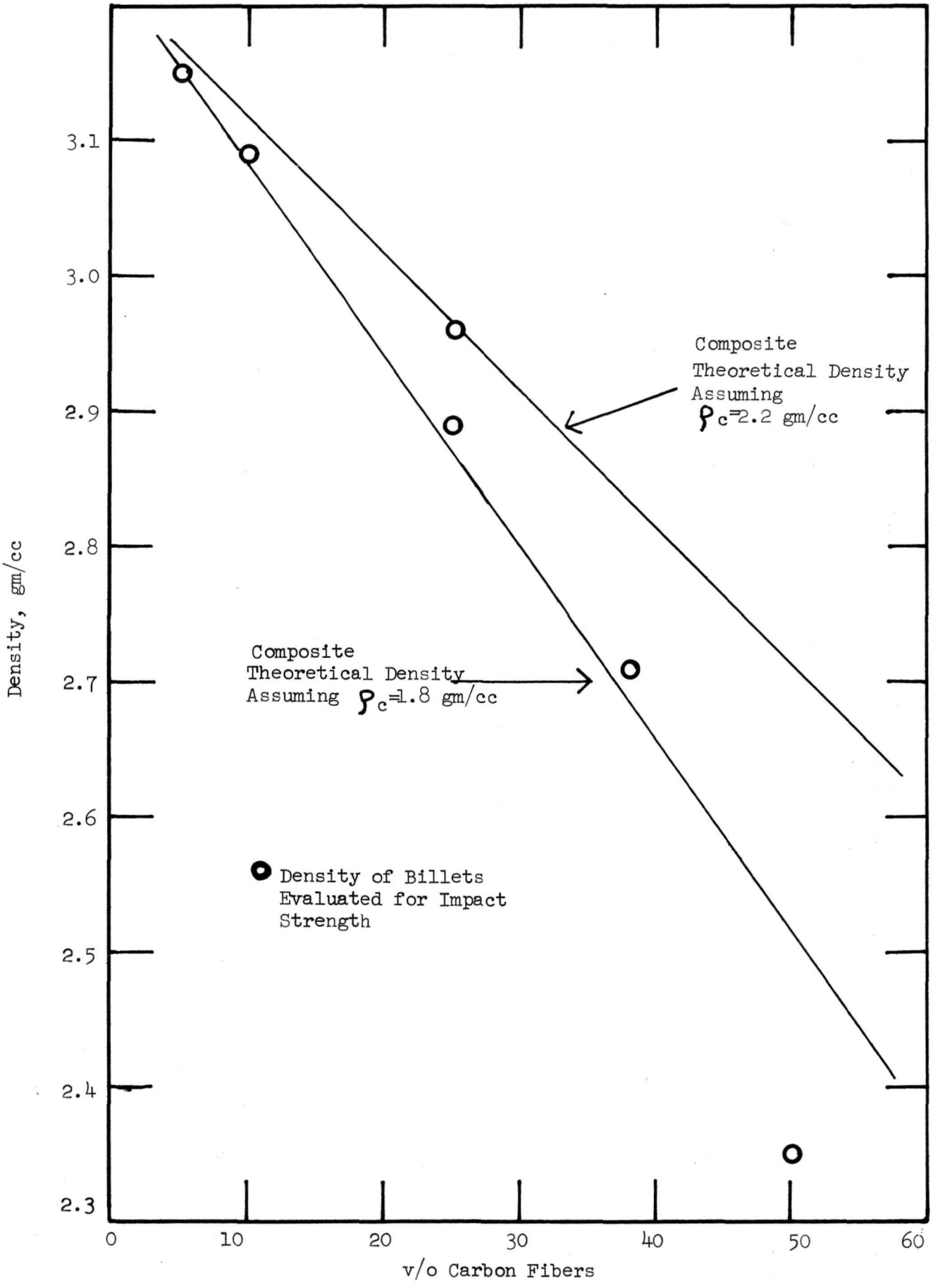

Figure 5. Density of SiC/C Billet Compared with Composite Theoretical Density

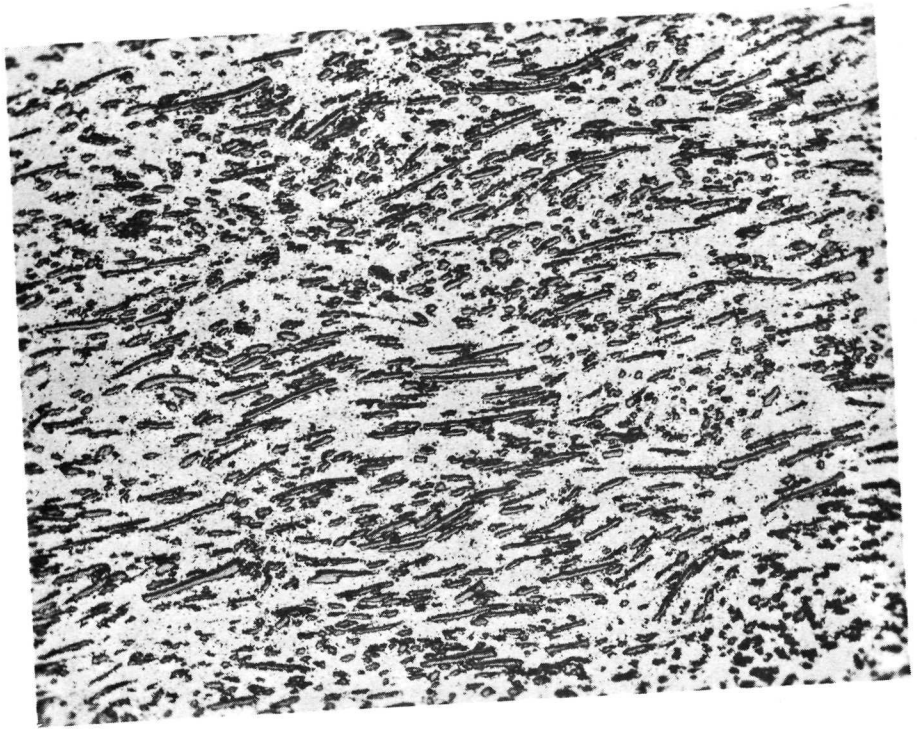

5486-1 (a) 75X

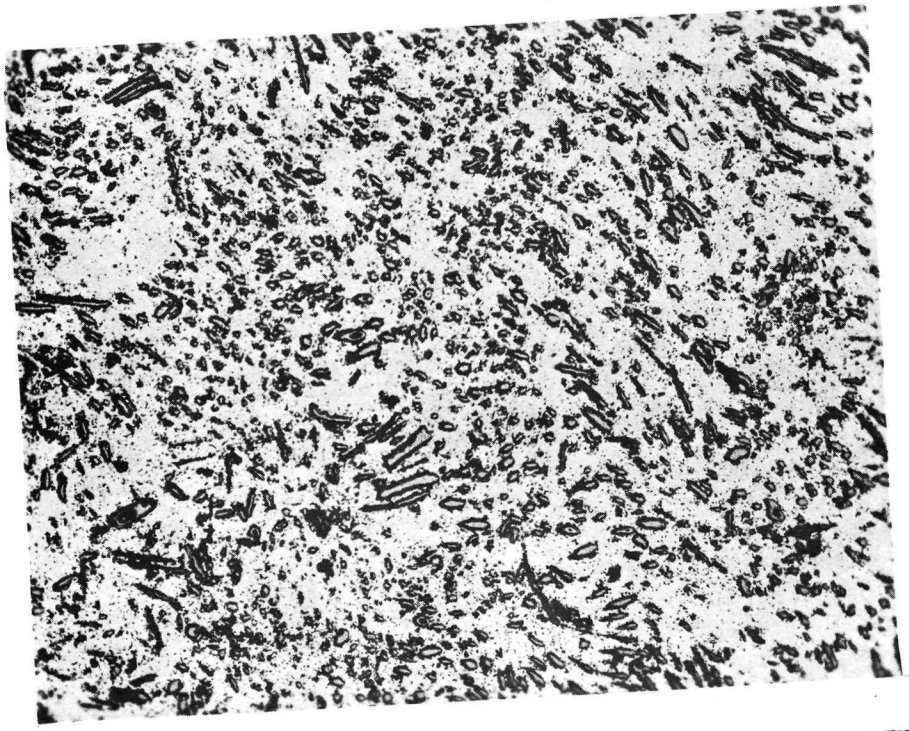

5486-2 (b) 75X

Figure 6. SiC plus 25 v/o Avco Carbon D1574 Showing Microstructure in Plane, (a) Perpendicular, and (b) Parallel to the Pressing Direction.

Several billets (D1583 and D1584) exhibited microstructures inferior to Figure 6. Non-uniform mixing and high porosity poxkets were observed. This may have been a result of incomplete fiber bundle dispersion with a high percentage of fiber bundles standing parallel to the pressing direction and thereby resisting densification. A lower viscosity slip was employed for billet D1592 and it was mixed 15 seconds longer for a total of 30 seconds. Billet D1594 and all billets subsequently produced (higher numbers) employed the above steps plus an ultrasonic distribution step. As shown in Figure 7, good fiber dispersion and alignment were achieved at the expense of some fiber break-up. The fibers were removed during etching of the structure for Figure 7b. The ratcheted interface demonstrates some matrix/fiber interaction and an apparently good bond when viewing 7a. The light etching revealed a 12 μm matrix grain size. In general, the structure was judged as satisfactory for mechanical evaluation, although widely spaced pore pockets were observed. Thus, the structure has not been optimized.

C. Silicon Nitride Base Systems

1. Silicon Nitride

a. Powder

The silicon nitride powder source was Advanced Materials Engineering, Ltd., as they are the only supplier of fine α-Si_3N_4. The alpha form was judged to be preferable to beta Si_3N_4, which had been used extensively on the previous program[ref. 1], because of the fine grain size, ease of fabrication, and improved strength properties.[ref. 10] α-Si_3N_4 is thought to be an oxygen containing compound of the composition $Si_{11.5}N_{15}O_{0.5}$ rather than a phase modification of β-Si_3N_4.[ref. 12] Three lots of this powder were received during this program. The initial lot (MRC) was purchased through Materials Research Corp., but it was manufactured by the same source. The X-ray characterization is given in Table V. Phase analyses were estimated by comparing X-ray diffraction peak intensities for α(110), β(110), Si_2N_2O(200) with the supplier analysis for the MRC lot. Thus, the relative ranking is accurate, but the precision of the analysis is questionable. This powder has been reported[ref. 11] to have between 1.2 and 2.3 wt. % impurities with Fe, Ca, Al, Ni, and Mg the major impurities.

Powder physical characterization studies were conducted on the MRC lot of Si_3N_4 powder in the as-received form and after ball milling for two periods of time--16 hours and 54 hours. The powders were examined by Coulter Counter and three direct observation techniques; the petrographic microscope, reflected light microscope, and electron microscope. Powder was embedded in plastic and polished for the reflected light examination. The electron microscopy results are illustrated in Figure 8. Both rods and nearly spherical shaped particles are apparent and measurements on the changes due to ball milling are given in Table VI.

The Coulter Counter was not capable of giving accurate results below 1 micron; thus, measurements with this instrument are representative of agglomerate size. Figure 9 illustrates the results of a ball milling experiment as well as data for two Si_3N_4 powder lots. The reduction in agglomerate size from approximately 9 μm to 2 μm for 54 hours of ball milling was confirmed by a reflected light microscopic study.

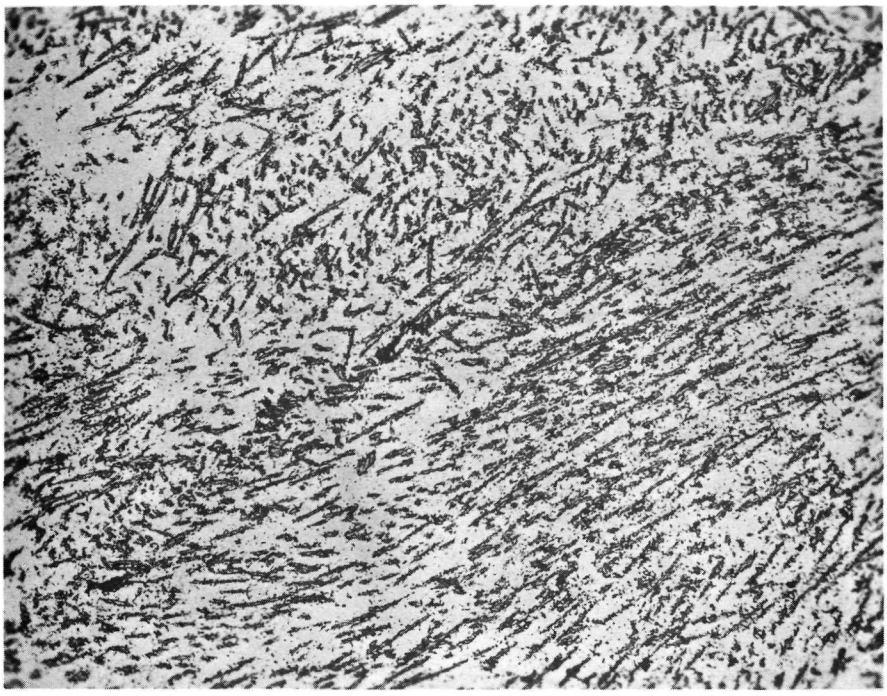

5512-4 (a) 100X

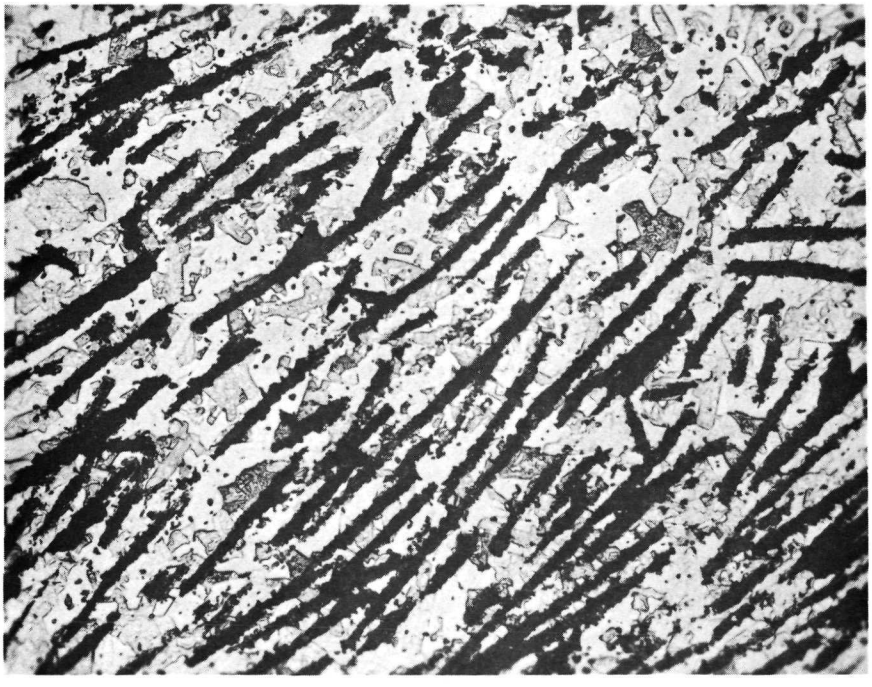

5512-6 (b) 250X

Figure 7. SiC plus 25 v/o Thornel 75, D1594, Showing Microstructure in Plane (a) Perpendicular, and (b) Parallel to Pressing Direction.

TABLE V

X-RAY ANALYSES OF Si_3N_4 POWDERS

	MRC	AME Lot 1	AME Lot 2
α Si_3N_4	Major	Major	Major
β Si_3N_4	Minor	Minor	Minor
Si_2N_2O	None	Trace	None
α Fe	None	Trace	Trace
Unidentified Phase	Present	Present*	None
α/β	5.68	9.75	3.00

*Separation techniques used, followed by X-ray analyses yield α Al_2O_3.

TABLE VI

MRC Si_3N_4 CRYSTALLITE SIZE

		Crystallite Size, Å	
Morphology	As-Received	16-Hr. Ball Mill	54-Hr. Ball Mill
Spherical	1000	750	775
Rod	900 x 12,000	990 x 7700	900 x 4700

71168 (a) 30,000X

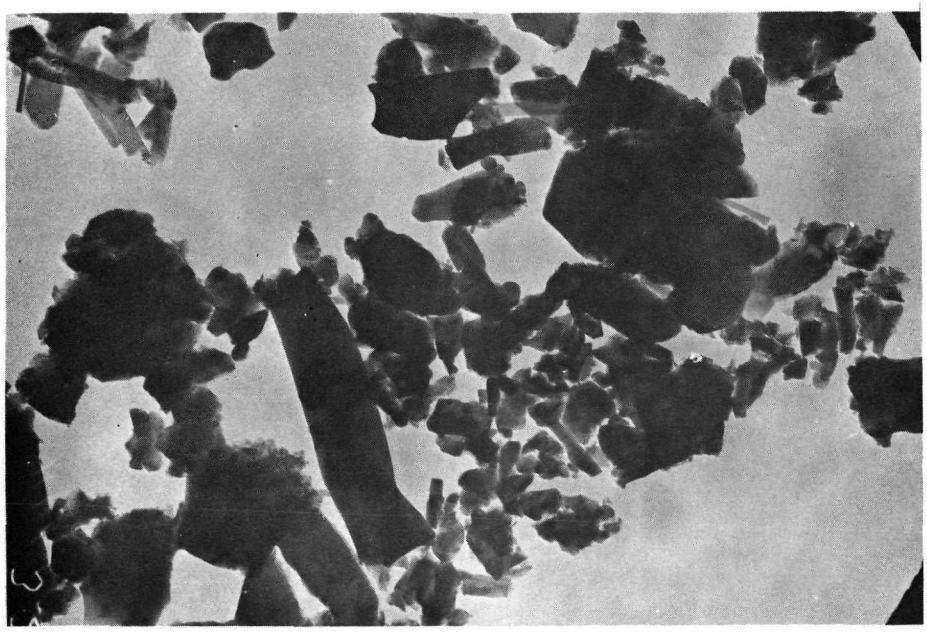

71174 (b) 30,000X

Figure 8. MRC Lot Si_3N_4 Powder (a) As-Received, and (b) After 54 Hours of Ball Milling.

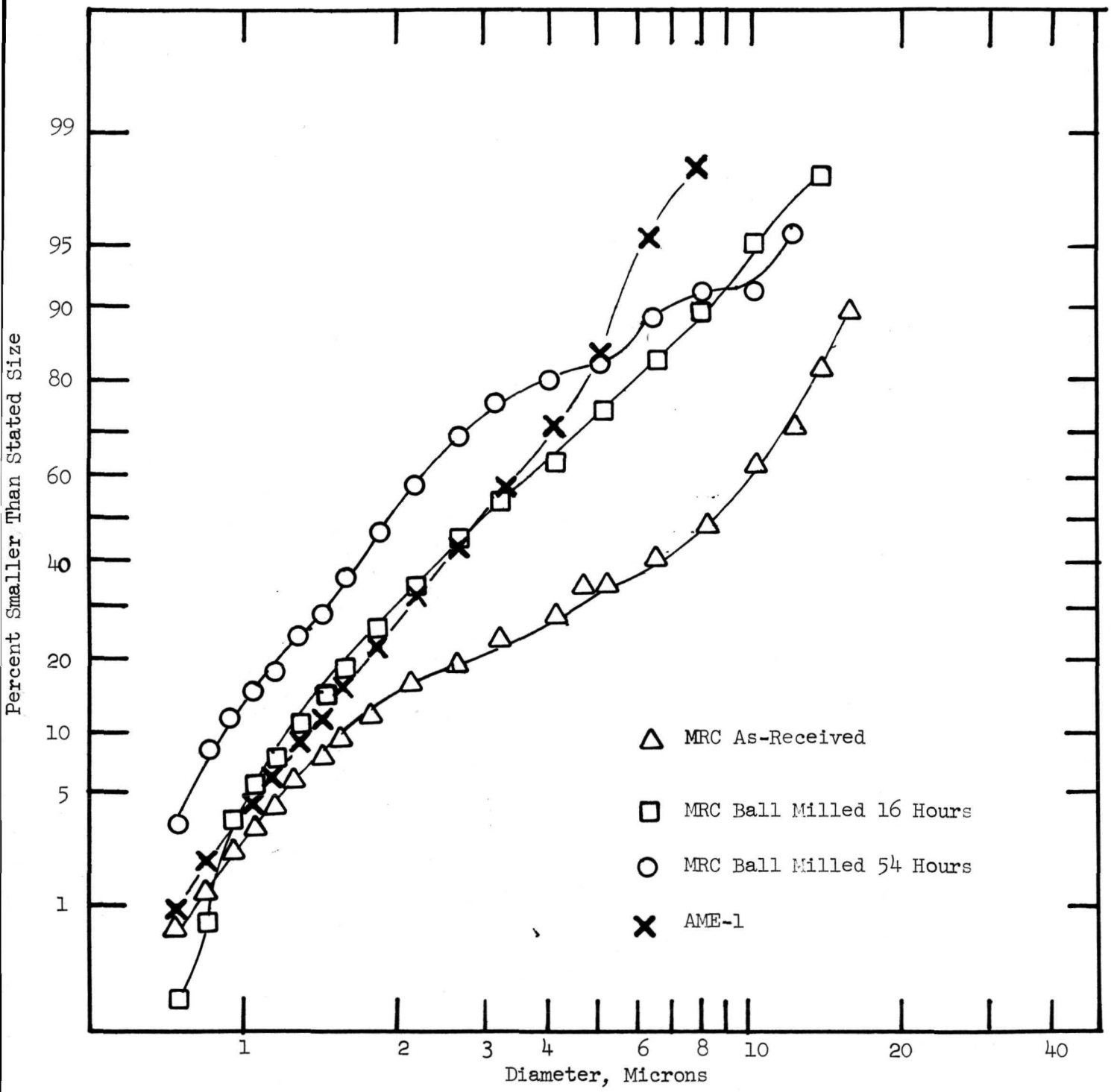

Figure 9. Agglomerate Size Distribution for -300 Mesh MRC and AME-1 Si_3N_4 Powder Showing the Effect of Ball Milling.

The reduction in crystallite size by ball milling was not thought to significantly enhance densification or properties. However, the reduction of agglomerates was judged worthwhile as improved mixing of the densification aid and reinforcement phases was expected.

A sieving separation and analysis experiment was conducted on the as-received AME-1 powder. It was found that 4 w/o consisted of hard agglomerates that would not easily pass a 325 mesh screen. In addition, organic fibers and two other isolations of foreign appearing particles were extracted. X-ray identification of the particles revealed α Fe and α Al_2O_3. The Al_2O_3 would probably form $MgAl_2O_4$ which has previously(ref. 1) been found to be an effective additive to Si_3N_4; thus, the presence of this phase was not particularly disturbing. α Fe particles were also found in AME-2 powder lot. The discrete particles of α Fe are worrisome as it is not difficult to visualize such particles forming strength limiting flaws in a finished billet. The powder was screened prior to use.

b. Consolidation

Previous work(ref. 1) employed 5 w/o of the MgO or $MgAl_2O_4$ densification additive. It was reasoned that a lower concentration might improve high temperature properties. Consequently, 1 w/o level of additive was employed for much of this program. Recently, Lange and Terwilliger(ref. 10) have shown that densification kinetics are markedly reduced with 1 w/o MgO compared with 5 w/o MgO. Table VII lists the hot pressing conditions and results for unreinforced Si_3N_4. The powder lot turned out to be an important variable, thus the results will be discussed by powder lot.

Pressings D1562 and D1563 using the MRC powder lot showed that a 96% relative density was achieved for both 100 and 140 minutes, respectively, at 3092°F (1973°K). Increasing the pressing temperature to 3182°F (2023°K) improved the bulk density slightly to 96.2%. However, a density of 97.9% was achieved in pressing 1595 by employing a step cycle of 75 minutes at 3092°F (1973°K) and 30 minutes at 3182°F (2023°K). It is thought that the improved densification noted in the step pressing was due to the phase change from α to β -Si_3N_4 under final stage consolidation conditions. Consequently, this cycle was employed for much of the remaining work.

Phases present in the hot pressed billets and starting powders are compared in Table VIII. Billet 1563 exhibited significant concentrations of α Si_3N_4 and Si_2N_2O. Extending the temperature 90°F was apparently sufficient to convert these two oxygen impurity phases to β -Si_3N_4. Grieveson, Jack, and Wild(ref. 12) believe the O^{-2} combines with Mg^{+2} and Si^{+4} to form vitreous $MgSiO_3$. This reaction is preceded by the formation of Mg_2SiO_4 from MgO and free SiO_2. Based on the apparently large amount of O in billet 1563 and the absence of enough α-Si_3N_4 in 1575 to identify by X-ray examination, it appears that some O_2 is being lost from the system as a gas phase. Differences in powder preparation may account for some of the difference in final O concentration and phase content. It was customary for Si_3N_4 to lose weight during hot pressing.

Powder lot AME-1 gave quite different densification behavior as

TABLE VII

FABRICATION CONDITIONS FOR Si_3N_4

Run No.	Material	Additive	Temp. °F	Temp. °K	Pressure psi	Pressure MN/m^2	Time min.	Density gm/cc	Density $Kg/m^3 \times 10^3$
D1562*	MRC Si_3N_4	1 w/o MgO	3092	1973	4000	27.5	100	3.07	3.07
D1563	MRC Si_3N_4	1 w/o MgO	3092	1973	4000	27.5	140	3.07	3.07
D1575*	MRC Si_3N_4	1 w/o MgO	3182	2023	4000	27.5	100	3.08	3.08
D1595*	MRC Si_3N_4	1 w/o MgO	3092	1973	4000	27.5	75		3.13
			3182	2023	4000	27.5	30	3.13	
D1599	MRC Si_3N_4	1 w/o MgO	3092	1973	4000	27.5	75		3.12
		2 w/o C	3182	2023	4000	27.5	30	3.12	
D1672	AME-1	1 w/o MgO	3092	1973	4000	27.5	75		2.81
	Si_3N_4		3182	2023	4000	27.5	65	2.81	
D1676	Repress 1672		3182	2023	4000	27.5	180	2.97	2.97
D1705*	AME-1	4 w/o MgO	3092	1973	4000	27.5	65		3.16
	Si_3N_4		3182	2023	4000	27.5	65	3.16	
D1716	AME-2	1 w/o MgO	3092	1973	4000	27.5	65		3.10
	Si_3N_4		3182	2023	4000	27.5	65	3.10	
D1725*	AME-2	1 w/o MgO	3092	1973	4000	27.5	65		3.12
	Si_3N_4		3182	2023	4000	27.5	65	3.12	
D1747*	AME-1 Si_3N_4	4 w/o MgO	3182	2023	4000	27.5	120	3.16	3.16
D1749	AME-2 Si_3N_4	4 w/o MgO	2912	1873	4000	27.5	60	2.80	2.80
D1750	Repress 1749		3002	1923	4000	27.5	70	3.16	3.16
D1755*	AME-2 Si_3N_4	1 w/o $MgAl_2O_4$	3092	1973	4000	27.5	65		3.16
			3182	2023	4000	27.5	65	3.16	
D1757	AME-3 Si_3N_4	1 w/o MgO	3182	2023	4000	27.5	120	3.17	3.17
858	AME-3 Si_3N_4	1 w/o MgO	3137	1998	3000	20.6	120	3.16	3.16

*Impact tested.

TABLE VIII

Correlation of Phases in Si_3N_4 Powder and Fabricated Billets

Powder Lot	Billet Number	Pressing Temp. °F	Pressing Time min.	Relative Theoretical Density	Grain Size microns	Powder Phases			Billet Phases		
						α	β	Si_2N_2O	α	β	Si_2N_2O
MRC	D1563 + 1% MgO	3092	140	0.963	0.7	85%	15%	0%	12%	69%	19%
	D1575 + 1% MgO	3182	100	0.965	1.3	85%	15%	0%	0%	93%	7%
AME-1	D1705 + 4% MgO	3182	65	0.991	1.7	88%	9%	3%	23%	77%	0%
AME-2	D1725 + 1% MgO	3182	65	0.978	1.0	75%	25%	0%	0%	99+%	0%

illustrated by the low density for pressing D1672. The billet was repressed to 3182°F (2023°K) for 180 minutes which raised the bulk density from 87.9% to 92.9%. However, pressing 1705 demonstrated that increasing the densification aid from 1 w/o to 4 w/o improved the kinetics markedly and 98.8% was achieved using the standard pressing cycle. About 23% α-Si_3N_4 was retained in pressing 1705 (Table VIII). It was somewhat surprising that Si_2N_2O was not found in 1705 as was experienced in pressings 1563 and 1575. Perhaps the larger MgO content tied up the excess oxygen from the most oxygen-rich phase as $MgSiO_3$.

The AME-2 powder lot behaved more like the original MRC powder lot. Densities of 97% and 97.5% were obtained for the standard cycle using 1% MgO additive compared with 97.9% for the MRC powder. Pressing D1749 and D1750 established that 98.8% density could be achieved as low as 3092°F (1923°K) using 4 w/o MgO additive. This information was useful for the reinforcement studies where minimum thermal cycles were desirable. As had previously been discovered(ref. 1), $MgAl_2O_4$ was a suitable densification aid. Run D1755 demonstrated that 1 w/o was sufficient to achieve 98.8% density.

Powder lot AME-3 was received near the end of the program and was used for one verification run (D1757) to assure that the densification behavior was similar to AME-2 and MRC lots and to fabricate a 9-inch by 9-inch by 3/8-inch plate for evaluation by NASA. Acceptable densities were achieved on both billets.

The decreased densification kinetics for powder lot AME-1 was examined in light of the characterization studies outlined in Section III.C.1.a. It was recognized that further powder characterization tests were possible, but it is thought that a reasonable explanation for the results can be offered based on the work conducted. Neither crystallite size, agglomerate size, nor Fe and Al_2O_3 impurity phases are thought to be responsible. Lot AME-1 had significantly higher α-Si_3N_4 content than the other two lots. It is postulated that the greater α-Si_3N_4 concentration in a powder lot, the greater is the tendency for Si_2N_2O formation. The X-ray results for AME-1 powder show Si_2N_2O, whereas it was not found in the other two lots. In the conversion of α-Si_3N_4 to β-Si_3N_4, some of the O^{-2} in α-Si_3N_4 combines with Mg^{+2} and Si^{+4} to form $MgSiO_3$. This phase must participate in the densification by a liquid phase pressure sintering mechanism with some solubility for Si_3N_4. (If this was not true, grain growth would not occur. Electron micrographs show the vitreous $MgSiO_3$ phase wets β-Si_3N_4.) With only 1 w/o MgO added (D1672), it is postulated that enough excess Si^{+4} and O^{-2} remain to in some way impede the densification process. A lower viscosity and diffusion constant for the grain boundary phase is predicted. The addition of 4 w/o MgO (D1705) is apparently sufficient to accommodate the excess O^{-2} of the Si_2N_2O phase first and then the α-Si_3N_4 in AME-1 and allow densification to proceed.

The results of this powder-additive, composition-processing cycle phase study are generalized and summarized in Table IX. These studies were not verified with duplicate samples and are expected to be dependent on oxygen partial pressure during consolidation, thus no effort was made to compare results with other investigations.

TABLE IX

EFFECT OF HIGH α-Si_3N_4 POWDER, COMPOSITION, AND PROCESS CYCLE ON BILLET PHASE ANALYSIS

	Variable	Expected Result
1.	Low (75%) α-Si_3N_4	Pure β-Si_3N_4 in billet
2.	Increased α in powder	Possibility of Si_2N_2O in powder
3.	Increased α + 1% MgO	Slow densification kinetics
4.	Increased α + 4% MgO	Improved densification; possibility of retained α in billet
5.	1% MgO	Possibility of α and Si_2N_2O in billet
6.	1% MgO - increased thermal cycle	Lose α-Si_3N_4 first; may retain Si_2N_2O
7.	Increase MgO	Increased grain growth

c. Microstructure

The microstructures were evaluated for billets fabricated from the three Si_3N_4 powder lots. The billets involved were further evaluated both for impact strength and stress rupture strength; consequently, the microstructures were also useful in interpreting the property data.

Figure 10 illustrates the as-polished and etched structure of D1563 fabricated at 3092°F (1973°K) with the MRC powder. The three reflectivities in Figure 10a probably represent the three phases found by X-ray analysis. The medium grey phase is β-Si_3N_4, but it is not possible to establish, based on the work conducted, the identity of the α-Si_3N_4 and Si_2N_2O phases. The large light patches are from 1-4 μm in diameter. It was not possible to establish whether or not these were single grains. The matrix grain size was about 0.7 μm as shown in Figure 10b. A large 4 μm grain could be a strength limiting feature but flaws nearer 50 μm have been predicted by Lange and Terwilliger(ref. 10). (The etching was accomplished with boiling 14 HF · 43 HNO_3 · 43 $C_3H_6O_3$.)

Figure 11 illustrates two sectional views of D1575 fabricated with the MRC powder lot. The etching of Figure 11a is not complete, but basically the structure looks similar to Figure 10b. The structure shown in 11b is nearly equiaxed indicating a lack of texture development in pressing. A lineal analysis of the parallel section gave a 1.3 μm grain size. The larger grain size compared with D1563 was undoubtedly due to the 90°F higher processing temperature.

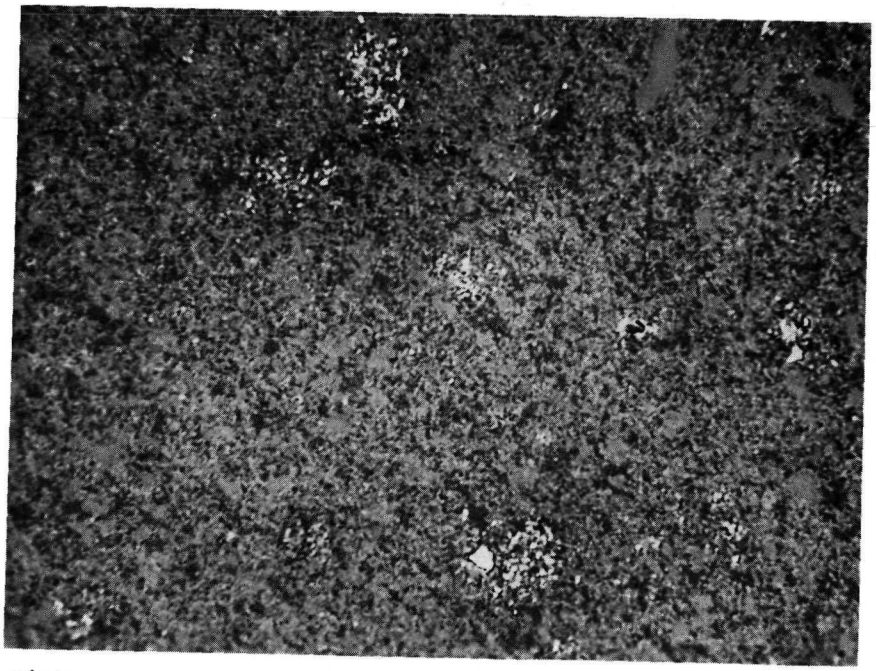

5470-3 (a) 750X

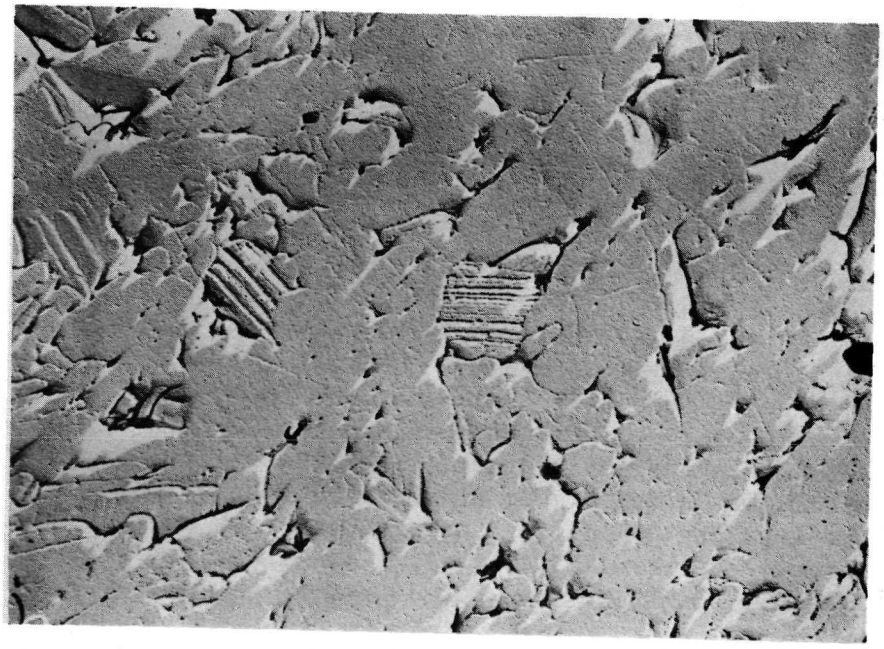

71338 (b) 15,000X

Figure 10. Si_3N_4 Specimen D1563 from MRC Powder Lot Showing (a) As-Polished Structure, and (b) Etched Structure with 0.7 μ Grain Size.

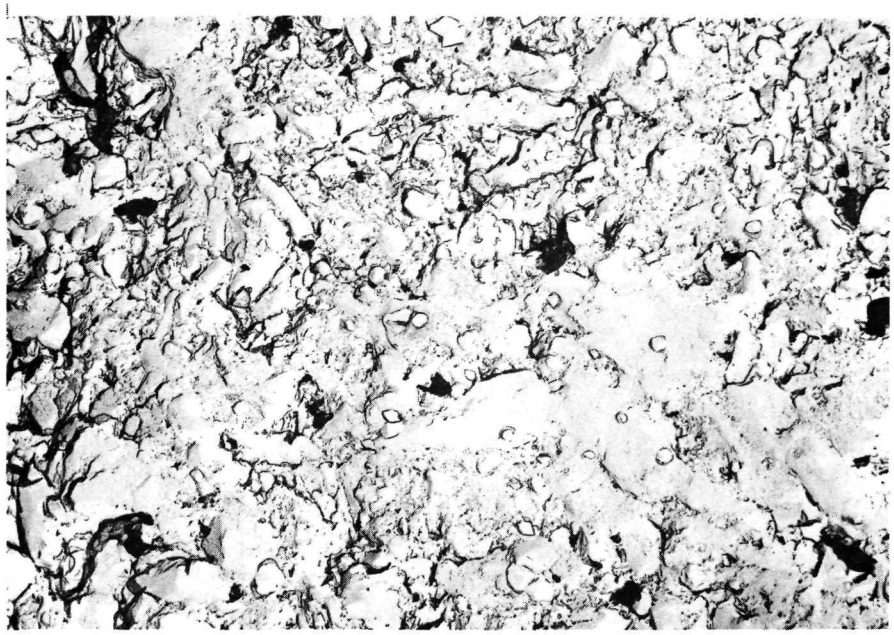

72335 (a) 7500X

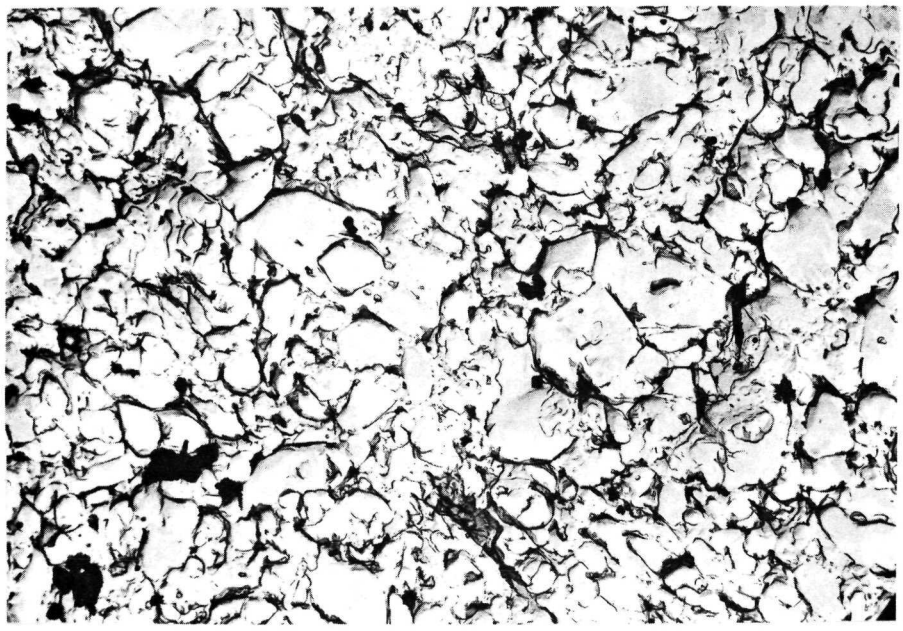

72333 (b) 7500X

Figure 11. Si_3N_4 Specimen D1575 from MRC Powder Lot Showing Etched Microstructure in Plane (a) Perpendicular and (b) Parallel to Pressing Direction.

Recalling that the AME-1 powder lot required 4% MgO addition to complete densification, it is not surprising to observe a wider apparent grain boundary phase for D1705 (Figure 12). The two different sectional views reveal quite different etched structures (using K_2CO_3 + NaF etch)(ref. 10) indicative of microstructural texturing. The texturing may result from a contribution of plastic deformation to densification or by alignment of the starting elongated particulates by particle sliding. The grain size at 1.7 μm is larger than either of the previous two samples discussed even though an equivalent temperature and 35 minute shorter pressing time was employed for this sample compared with D1575. Since the starting crystallite sizes were equal, it was concluded that the higher MgO concentration promoted grain growth.

The structure of D1725 pressed from AME-2 powder is illustrated in Figure 13. The grain size has a duplex distribution although, on the average, the grain size is 1.0 μm which is logical when compared with the 1.3 μm for D1575 pressed at the same temperature 35 minutes longer. Some microstructural texturing has taken place as illustrated most clearly by the fine structure in Figure 13b. Note the thinner grain boundary film for this sample compared with D1705. This is a result of using 1% MgO compared with 4% MgO for D1705.

The Si_3N_4 microstructure appears to be a strong function of the starting powder phase analysis, the concentration of the additive and the process thermal cycle. The achievement of reproducible structures will depend on careful control of all three major variables. The expected effects are included in Table IX.

2. Silicon Nitride Plus Silicon Carbide Whiskers

a. Silicon Carbide Whiskers

The National Research Division SiC whiskers described in Section III.B.2 were employed in all but one of the billets fabricated in this system. Carborundum SiC whiskers were employed for the remaining billet as it was of interest to fabricate one billet with reduced whisker dimensions.

b. Consolidation

Table X lists the Si_3N_4 + SiC whisker billets. Billet D1752 was fabricated with the fine Carborundum SiC whiskers while all others contain the coarse National Research Division SiC whiskers.

Since the theoretical densities of Si_3N_4 and SiC are so close, a value of 3.20 gm/cc is a close approximation of the theoretical density for billets in this system. Table X shows that the fabricated bulk density is inversely proportional to the volume percent whisker additive. D1619 containing 50 v/o SiC whiskers was only 90% dense. This level of density was judged unsuitable for mechanical evaluation.

SiC whiskers caused slow densification kinetics when added to SiC as discussed in Section III.B.2. Certainly they could be expected to interfere with the Si_3N_4 densification to an even greater extent since Si_3N_4 is fabricated about 750°F (399°K) lower than SiC. In addition to limiting the transport of Si_3N_4 by the liquid phase, whiskers oriented parallel

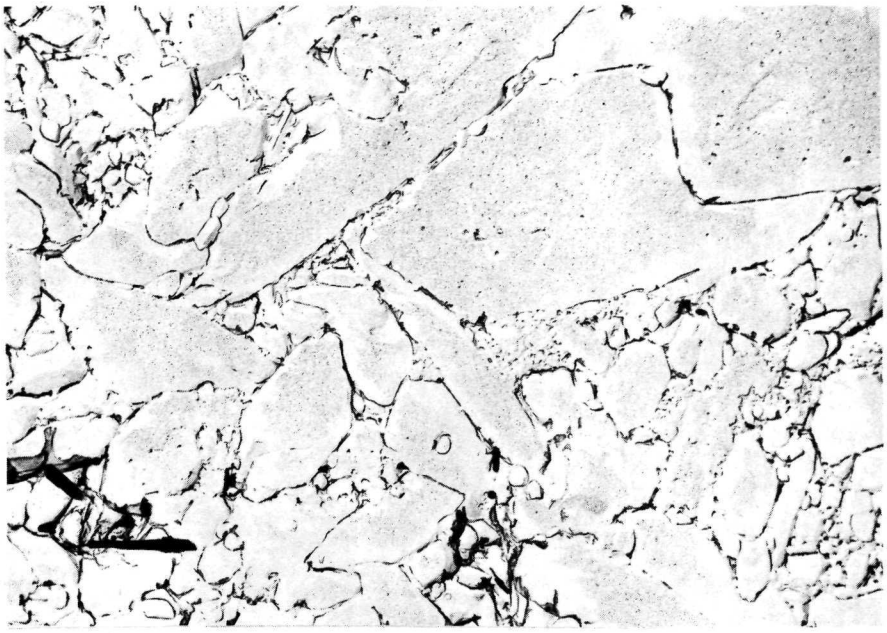

72339 (a) 7500X

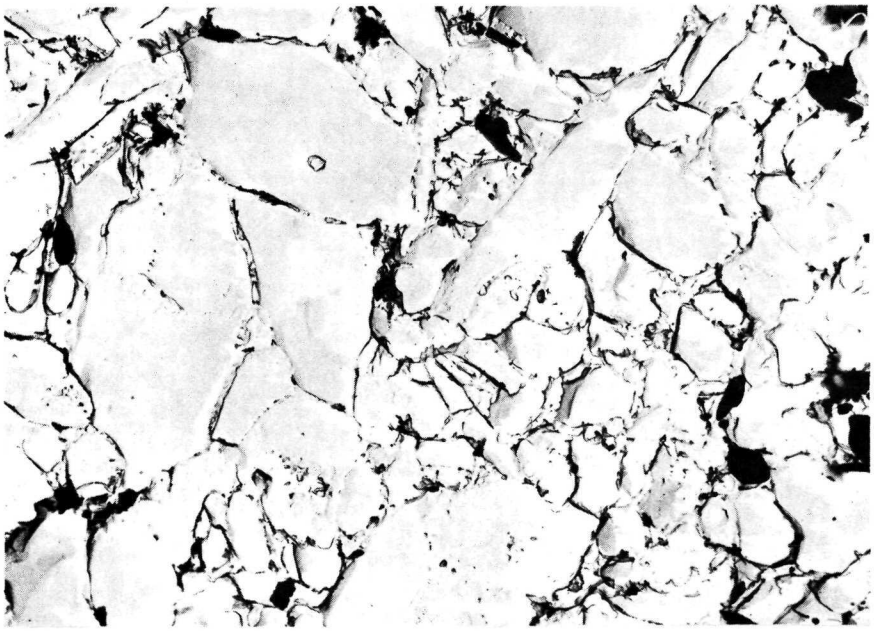

72337 (b) 7500X

Figure 12. Si_3N_4 Specimen D1705 from AME-1 Powder Lot Showing Etched Microstructure in Plane (a) Perpendicular and (b) Parallel to Pressing Direction.

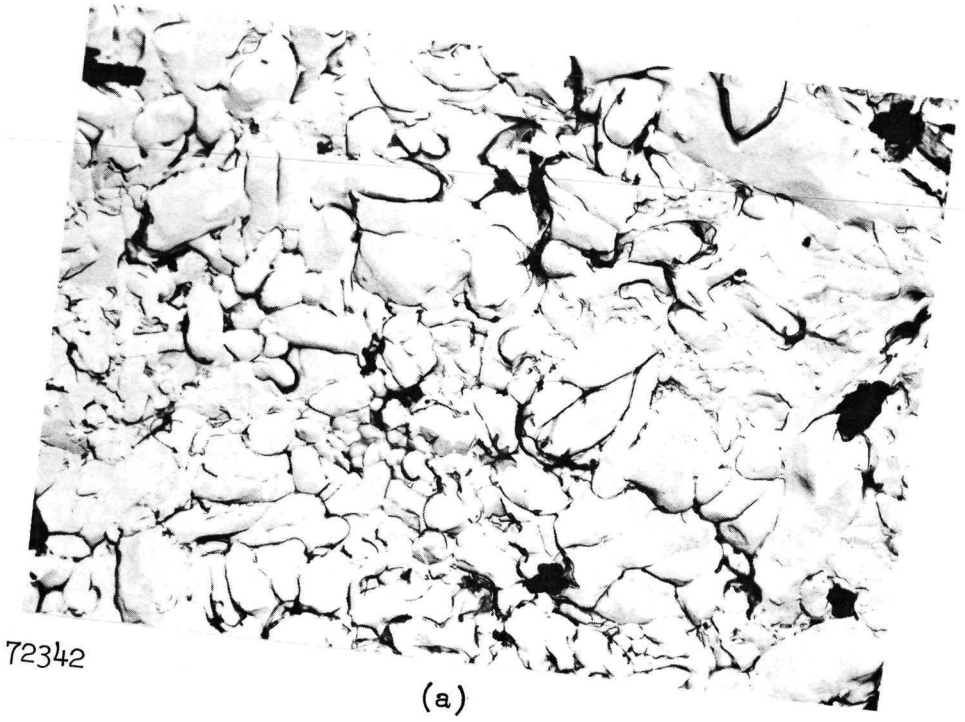

72342

(a)

7500X

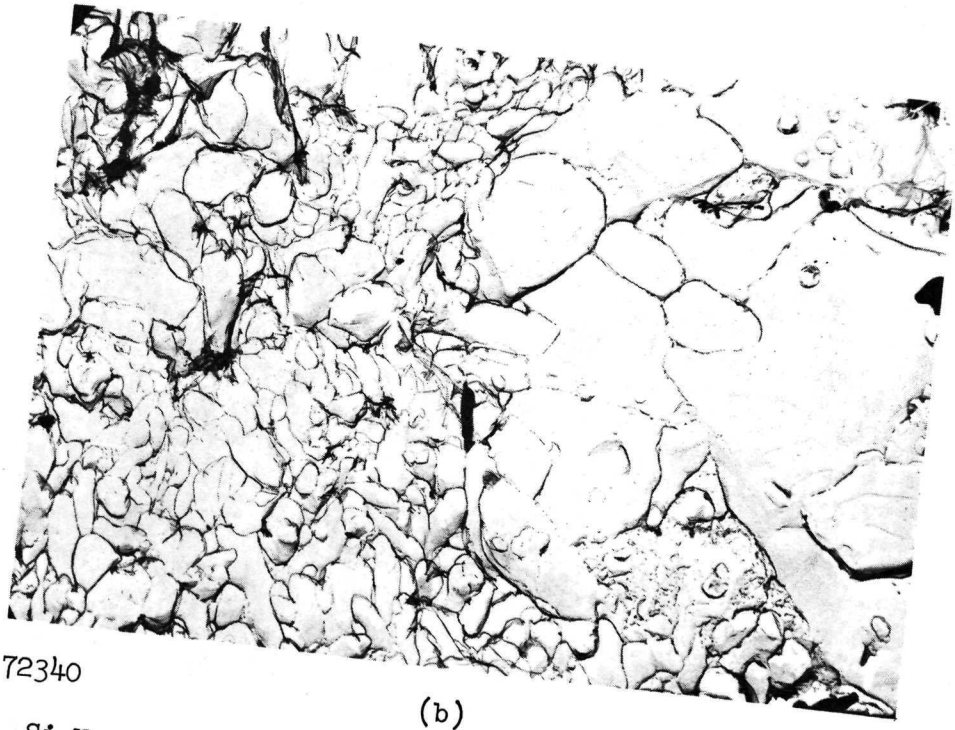

72340

(b)

7500X

Figure 13. Si_3N_4 Specimen D1725 from AME-2 Powder Lot Showing Etched Microstructure in Plane (a) Perpendicular, and (b) Parallel to Pressing Direction.

TABLE X

Fabrication Conditions for the Si_3N_4 Plus SiC Whisker System

Run‡ No.	Material	Additive	Temp. °F	Temp. °K	Pressure psi	Pressure MN/m^2	Time min.	Density gm/cc	Density $Kg/m^3 \times 10^3$
D1734*	AME-2 Si_3N_4	1 w/o MgO 5 v/o SiC	3092 3182	1973 2023	4000 4000	27.5 27.5	65 65	3.15	3.15
D1729*	AME-2 Si_3N_4	4 w/o MgO 10 v/o SiC	3092 3182	1973 2023	4000 4000	27.5 27.5	65 65	3.12	3.12
D1752*	AME-2 Si_3N_4	1 w/o MgO 10 v/o fine SiC	3092	1973	4000	27.5	95	2.79	2.79
D1752B	Repress 1752		3182	2023	4000	27.5	130	3.13	3.13
D1606*	MRC Si_3N_4	1 w/o MgO 38 v/o SiC	3092 3182	1973 2023	4000 4000	27.5 27.5	75 30	3.00	3.00
D1619	MRC Si_3N_4	1 w/o MgO 50 v/o SiC	3092 3182	1973 2023	4000 4000	27.5 27.5	75 30	2.58	2.58
D1668	MRC Si_3N_4	1 w/o MgO 50 v/o SiC	3092 3182	1973 2023	4000 4000	27.5 27.5	75 75	2.71	2.71
D1668	Repress Si_3N_4	1 w/o MgO 50 v/o SiC	3092 3182	1973 2073	4000 4000	27.5 27.5	75 75	2.88	2.88

*Impact tested

‡All billets fabricated with coarse National Research Division SiC whiskers except billet D1752, which was fabricated with fine Carborundun SiC whiskers.

or at some angle less than about 80° to the pressing direction would give mechanical resistance to the densification process. Orientation was achieved both in the cold forging step and hot pressing, but the statistics, of course, favor increased "end on" whisker resistance at the higher volume loadings.

Billets of the 5, 10, and 38 v/o SiC whisker compositions were judged sound and of a quality worthy of mechanical evaluation.

c. Microstructure

Billet 1729 contained 10 v/o SiC and was 99.2% dense after consolidation. Figure 14a illustrates an area in the cross section where a large pore cavity was found. The structure around the cavity suggests a severe vaporization or melting reaction as the cause of the pore. The majority of the section possessed the dense aligned structure shown in Figure 14b, which was as good a structure as observed for any Si_3N_4/SiC whisker composite. However, it was recognized that in a brittle material, pores such as those shown in Figure 14a could act as strength limiting flaws cancelling any advantage of the whiskers. Many whiskers fractured during processing, which reduced the L/D ratio by factors of 1/3 and 1/2. A high reflectivity particulate phase was observed within the Si_3N_4 matrix. This phase has not been identified for these billets, but similar appearing phases found in unreinforced Si_3N_4 were identified as Si_2N_2O. Lange and Terwilliger(ref. 10) found somewhat similar phases in Si_3N_4 to be rich in Ca or Fe plus Si and reasoned that silicides were likely identifications.

3. Silicon Nitride Plus Silicon Nitride, Silicon Dioxide, or Carbon Fibers

a. Silicon Nitride Fibers

Three sources of silicon nitride fibers or whiskers were located; General Technologies Laboratory (GTL), Advanced Materials Engineering, Ltd. (AME), and the British Ministry of Defense Explosives Research and Development Establishment (ERDE). The latter two sources were found near the end of the program which precluded extensive consideration and incorporation of their fibers into composites.

Si_3N_4 fiber samples were ground and examined by the X-ray diffractometer technique. The GTL fibers were examined both in the as-received condition and after heat treating for 1 hour at 1673°K in H_2. The heat treatment was conducted to crystallize the as-received amorphous material. The results summarized in Table XI indicated that both the AME and ERDE whiskers are phase pure, but the GTL fibers appear to have not only O^{-2} impurity, but Mg^{+2} and Al^{+3} as well. The presence of an amorphous SiO_2 sheath was recognized by Cunningham and Shaver in their original description of this material(ref. 13).

The GTL fibers were formed through gas transport reactions, and are circular in cross section with uniform diameters of between 1 and 20 microns and from 15 microns to 15 inches long. The long fibers typically possessed an average tensile strength of 720 Kpsi when tested with a $\frac{1}{4}$-inch gage length and 405 Kpsi using a 1-inch gage length.(ref. 13) The maximum and

5584-1 (a) 50X

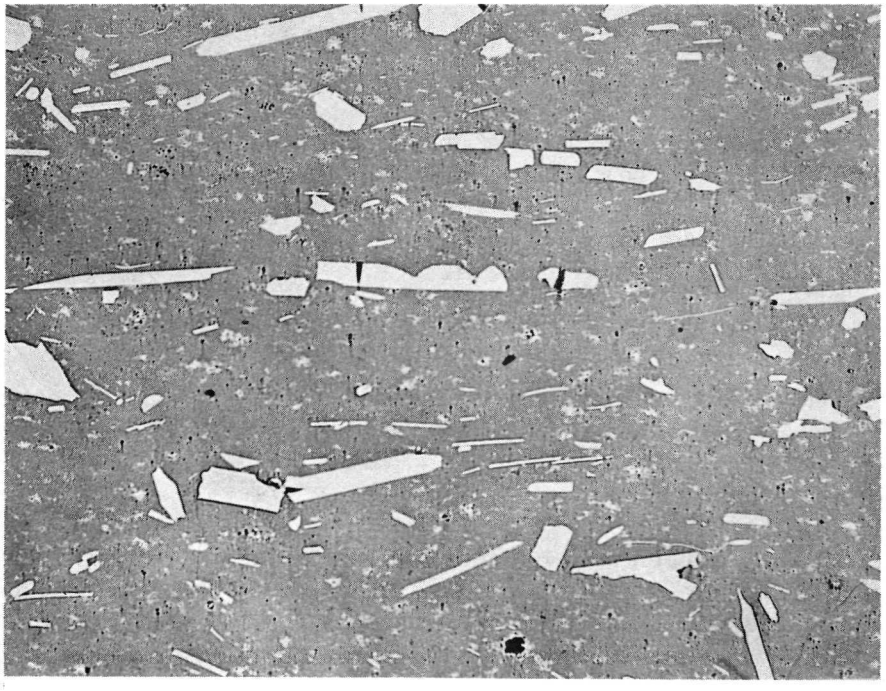

5584-3 (b) 100X

Figure 14. As-Polished Structure of D1729, Si_3N_4 + 10 v/o SiC Viewing Plane Parallel to Pressing Direction Showing (a) Large Pore Cavity, and (b) Structure for Major Fraction of the Area.

TABLE XI

X-RAY STUDY OF SILICON NITRIDE FIBERS

Phase Concentration	Source and Phase: GTL As-Received	GTL Heat Treated	AME As-Received	ERDE As-Received
Major	Amorphous	Cristobalite SiO_2	α Si_3N_4	α Si_3N_4
Minor	α Si_3N_4	α Si_3N_4 $Mg_2Al_4Si_5O_{16}$ Amorphous SiO_2	None	β Si_3N_4

minimum strengths recorded were 1500 Kpsi and 155 Kpsi, respectively. The measurement of elastic modulus appeared too inaccurate for quotation.

In addition to the question of phase purity, the GTL fibers were contaminated with black particulates which were identified as highly crystalline graphite. One billet was prepared with as-received fibers and a second was fabricated from fibers which had undergone an extensive separation and ultrasonic cleaning process.

b. Silicon Dioxide Fibers

Amorphous SiO_2 fibers were obtained from the J.P. Stevens Co. The fibers are 10 μm diameter and were chopped to 0.635 cm lengths.

c. Carbon Fibers

SiC coated carbon was obtained from Carborundum and examined microstructurally. Only 10-30% of the fibers in a bundle were coated which led to the conclusion that this material would be unsatisfactory. No other commercial sources of suitable material were found.

Thornel 75 (described in Section III.B.3) was chopped into 0.635 lengths and incorporated into composites.

d. Consolidation

As noted in Table XII, which lists the Si_3N_4 plus Si_3N_4, SiO_2 or

TABLE XII

Fabrication Conditions for the Si_3N_4 Plus Si_3N_4, SiO_2, or C Systems

Run No.	Material	Additive	Temp. °F	Temp. °K	Pressure psi	Pressure MN/m^2	Time min.	Density gm/cc	Density $Kg/m^3 \times 10^3$
1664*	MRC Si_3N_4	1 w/o MgO	3092	1973	4000	27.5	75	3.05	3.05
		25 v/o Si_3N_4	3182	2023	4000	27.5	30		
D1748*	AME-2 Si_3N_4	1 w/o MgO	3092	1973	4000	27.5	65	2.99	2.99
		20 v/o Si_3N_4	3182	2023	4000	27.5	75		
D1753	AME-2 Si_3N_4	4 w/o MgO 10 v/o SiO_2	3002	1923	4000	27.5	65	2.99	2.99
D1610*	MRC Si_3N_4	1 w/o MgO 25 v/o C	3092	1973	4000	27.5	15	2.59	2.59
D1662	MRC Si_3N_4	1 w/o MgO 25 v/o C	3092	1973	4000	27.5	75	2.28	2.28
D1669	MRC Si_3N_4	1 w/o MgO 25 v/o C	3182	2023	4000	27.5	15	2.14	2.14

*Impact Tested

C fiber billets, two pressings were made with Si_3N_4 fibers. The GTL fibers were incorporated into both billets with D1748 being the billet which contained the cleaned fibers. Preparation of the preform was very difficult due to the long fiber lengths. D1664 was 95.6% dense, whereas D1748 was 93.8% dense. As observed for previous composite systems, fibers retard the densification process.

D1753 was the only billet fabricated with chopped amorphous SiO_2 fibers. It was 96.6% dense (3.10 gm/cc theoretical density for the composite).

Pressing D1610 with a 25 v/o addition of Thornel 75 to Si_3N_4 was conducted under an abbreviated 1700°C pressing cycle to minimize the reaction to form N_2. The 2.59 gm/cc density achieved was about 91% dense (uncertainty due to the unknown density of carbon after hot pressing). Pressings D1662 and D1669 were of the same composition, but were conducted under different time/temperature cycles to ascertain if a higher density could be achieved. The relative densities were 80 and 75%, respectively, and weight losses of 46% and 31% were recorded for D1662 and D1669. This lends some confirmation to the interpretation of the N_2 reaction previously predicted(ref. 1) and accounts for the difficulty in obtaining high density.

e. Microstructure

Billet D1748 containing 20 v/o cleaned Si_3N_4 fibers has the as-polished structure shown in Figure 15. The structure is strongly textured. Mixing is not complete, although fibers are dispersed throughout the matrix. The porosity level appears lower than the calculated 6% which is probably due to the fibers having a lower theoretical density than the 3.20 gm/cc of Si_3N_4. Some chemical interaction took place during fabrication based on the irregular fiber/matrix boundary. This observation is consistent with the fiber phase analysis showing the presence of SiO_2. The structure of Billet D1664 fabricated with uncleaned Si_3N_4 fibers was very poor, showing reaction zones, large pore cavities, and some dense zones very similar to Figure 15.

The as-polished structure of D1753 containing 10 v/o chopped SiO_2 fibers is illustrated in Figure 16. The fiber morphology was lost during processing indicating a considerable chemical interaction. The large pore nests may be a partial result of this interaction. The overall structure was judged poor and not worthy of mechanical evaluation.

Billet D1610 was the densest in the Si_3N_4/C fiber system. The microstructure of this sample is shown in Figure 17. The fibers are non-uniformly dispersed leaving islands of dense Si_3N_4 matrix. Considerable porosity is in evidence. Figure 17b demonstrates that the carbon has not been completely consumed although considerable erosion is in evidence. The bonding looks quite tight at some of the Si_3N_4/C interfaces although others do not look quite as promising. Differential polishing rates between duo-hardness phases may account for some of the appearance of poor bonding. This billet was evaluated mechanically in spite of the poor structure.

4. Silicon Nitride Plus Metal Additions

a. Molybdenum

Thermodynamic calculations(ref. 1) showed that Mo and Cr should be

5608-4

50X

Figure 15. Si_3N_4 Plus 20 v/o Si_3N_4 Fibers, D1748, Showing Plane Parallel to Pressing Direction.

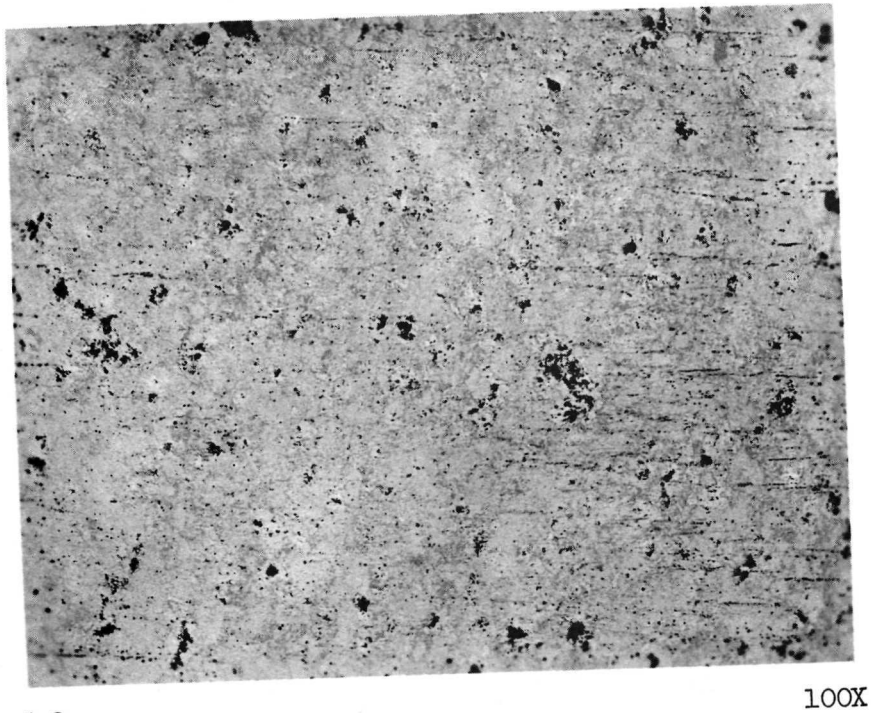

5608-3

100X

Figure 16. Si_3N_4 Plus 10 v/o SiO_2 Fibers, D1753, Showing Plane Parallel to Pressing Direction.

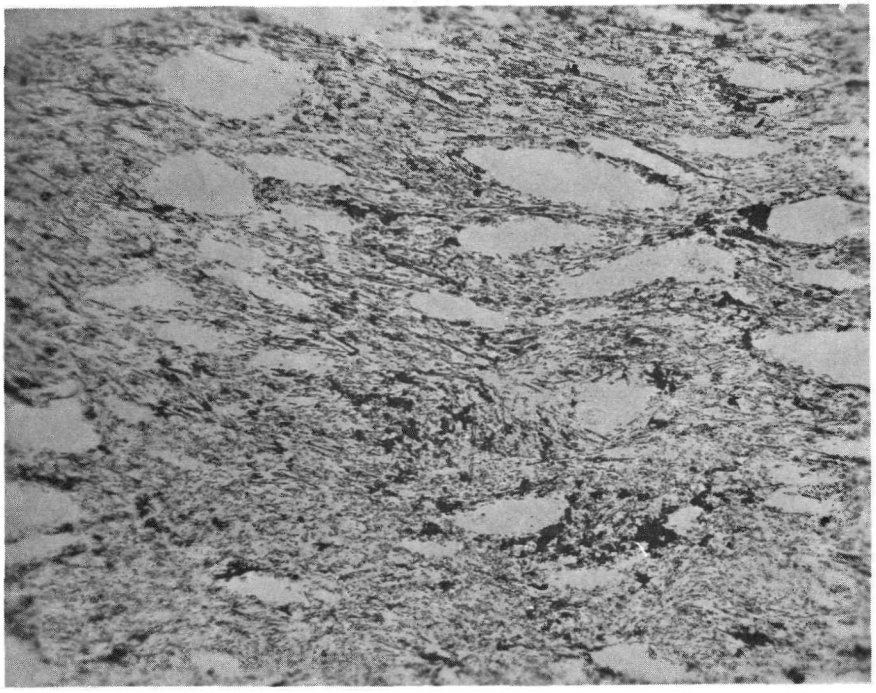

5540-1 (a) 50X

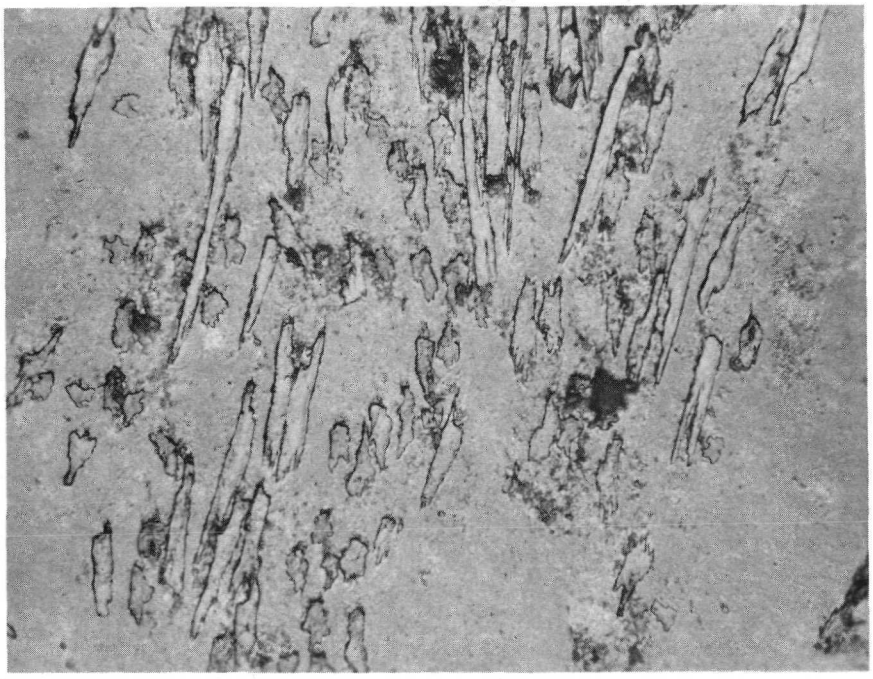

5540-2 (b) 500X

Figure 17. Si_3N_4 Plus 25 v/o C, Thornel 75, D1610, (a) Viewing Plane Parallel to the Pressing Direction, and (b) Si_3N_4/C Interactions.

stable with respect to their nitride at 3272°F (2073°K). The necessary thermodynamic quantities for calculation of stability against silicide formation were not available. Metallography on a test billet (D1685) containing Mo as well as other wires indicated that a central core of a 0.010 inch diameter Mo wire remained unreacted through the standard process cycle.

Thus, by employing one of the abbreviated Si_3N_4 densification cycles discussed in Section III.C.1.b., it was thought possible to retain some unreacted Mo. Wire 0.005 inch diameter was chopped into $\frac{1}{4}$-inch lengths for incorporation into a Si_3N_4 powder charge by the standard slip casting preform preparation process.

b. Rhenium

A trial pressing employing 0.005 and 0.010 diameter Re wires looked quite promising. Metallographic sections of the 0.005 inch diameter wire were interpreted as exhibiting only a 8 micron reaction zone for material hot pressed by the standard cycle which qualifies Re as more stable than either W or Mo in the presence of Si_3N_4. Wire 0.005 inch diameter was chopped into $\frac{1}{4}$-inch lengths for incorporation into a Si_3N_4 billet.

c. Chromium

Chromium was the second metal that was stable with respect to nitride formation.(ref. 1) The melting point of Cr is 3434°F (2163°K) which is slightly above the temperature where α-Si_3N_4 will densify. Chromium powder with an average particle size of 50 µm was employed for the one billet fabricated in this system.

d. Nichrome

It was decided to attempt fabrication employing a model superalloy recognizing the fact that it would melt during fabrication of the Si_3N_4. Ni20Cr, used for this study, has a melting point of 2550°F (1663°K). Billets were made employing a 90 µm particle size powder and one billet had as an additive phase 0.005 inch diameter Ni20Cr wire chopped into $\frac{1}{4}$-inch lengths.

e. Consolidation

Hot pressings containing metal additives are listed in Table XIII. Pressing D1685 contained strands of the candidate metal wires Re, Mo, and W. The results of this pressing have been referred to in the discussion on selection of metal additives. The W wires were more completely reacted than even Mo, which is surprising in view of the melting points of the two metals, but consistent with the thermodynamic calculations.(ref. 1)

The initial pressing with Mo wires (D1751) was badly laminated. The next pressing, D1760, was conducted 50°K higher and the pressure application and removal cycle were altered. These changes resulted in a sound billet which was slightly in excess of 100% of the theoretical density of the 5 v/o Mo composition. X-ray diffraction analysis revealed that some of

TABLE XIII

Fabrication Conditions for Si_3N_4 Plus Metal Additions

Run No.	Material	Additive	Temp. °F	Temp. °K	Pressure psi	Pressure MN/m^2	Time min.	Density gm/cc	Density $Kg/m^3 \times 10^3$
D1685	AME -2 Si_3N_4	1 w/o MgO Re, Mo, W	3182	2023	4000	27.5	120	3.31	3.31
D1751	AME-2 Si_3N_4	4 w/o MgO 5 v/o Mo	3092	1923	4000	27.5	65	2.99	2.99
D1760*	AME-3 Si_3N_4	4 w/o Mg 5 v/o Mo	3092	1973	4000	27.5	65	3.57	3.57
D1743*	AME-2 Si_3N_4	1 w/o MgO 1.7 v/o Re	3092	1973	4000	27.5	65	3.38	3.38
D1721*	AME-2 Si_3N_4	1 w/o MgO 5 v/o Cr	3092	1973	4000	27.5	65	3.33	3.33
D1719*	AME-2 Si_3N_4	1 w/o MgO 5 v/o Ni20Cr	3092	1973	4000	27.5	65	3.25	3.25
D1731*	AME-2 Si_3N_4	1 w/o MgO 10 v/o Ni20Cr	3092	1973	4000	27.5	35	3.10	3.10
D1761*	AME-3 Si_3N_4	4 w/o MgO 10 v/o Ni20Cr	3092	1973	4000	27.5	65	3.17	3.17

*Impact Tested

the Mo had reacted to form Mo_5Si_3 and Mo_2C, but some Mo remained. β-Si_3N_4 was the major phase, and about 10% α-Si_3N_4 remained. The abbreviated hot pressing cycle favored α-Si_3N_4 retention.

The Re containing billet (1743) was 97.2% of theoretical density. Only a small amount of wire was available, so the volume loading was only 1.7%. The mixing was not uniform, but the billet was sound and otherwise of sufficient quality for further evaluation. X-ray analysis on this billet found unreacted Re and ReSi. The α-Si_3N_4 content was estimated as 20%.

The pressing with Cr or Ni20Cr densified readily to >95% of theoretical. The fact that the metal phase was molten during pressing did not cause difficulty in die extraction or obtaining sound billets. Each of the billets was examined by X-ray diffraction. In 1721 containing 5 v/o Cr, the phase Cr_5Si_3 was identified as the only phase present other than silicon nitride. The Nichrome bearing billets contained one or more phases which could not be positively identified, but could be Ni, Ni_3Si, Ni_3Cr, $Ni_3(CrSi)$, Ni_3N, NiC, Ni_3C, or Cr. It was thought that Ni_3Si was the best identification and based on the identification of Cr_5Si_3 for D1721, this appears logical.

f. Microstructure

The structure of D1760 containing 5 v/o Mo wire is shown in Figure 18. The structure has been etched to illuminate the phase boundaries within the original Mo wires. These etched grains have a 575 Knoop hardness, whereas the remainder of the high reflectivity core is 1350 Knoop and the outer 15 μm sheath has a hardness of 1540 Knoop. Annealed Mo has a hardness of 240 Knoop, $MoSi_2$ is between 1290-1470 Knoop, and Mo_2C is 2000 Knoop.(ref. 14,15) Combining this analysis with the X-ray analysis, it is thought that the central grains are Mo solid solution hardened with Si and C and the remainder of the high reflectivity core is Mo_5Si_3, which leaves Mo_2C as the identification for the sheath. All these phases are quite brittle as noted by the tendency for cracking during preparation of the metallographic section. A crack was observed to pass through several wires and finally end in one wire. This behavior was a major goal of this approach. The thermal expansion mismatch did not appear to result in matrix cracking, although it is uncertain whether or not some of the wire cracks were a result of this effect.

Re wires were less reactive than Mo as illustrated in Figure 19. The microhardness for the central zone averaged 660 Knoop which is compared with 270 Knoop for annealed and 825 Knoop for swagged Re rod.(ref. 14) The outer zone of the wire had a hardness about 1300 Knoop. These results combined with the X-ray analysis lead to the conclusion that the central zone was unreacted Re. There was no microcracking in the billet. The low v/o Re available, combined with the large density difference in the phases, resulted in a non-uniform wire dispersion of this billet.

The microstructure of the Si_3N_4 billet containing 5 v/o Cr is illustrated in Figure 20. The Cr was inhomogeneously distributed and either melted, reacted, or pulled out during polishing. The X-ray findings of completely reacted Cr, along with the poor microstructure, led to the

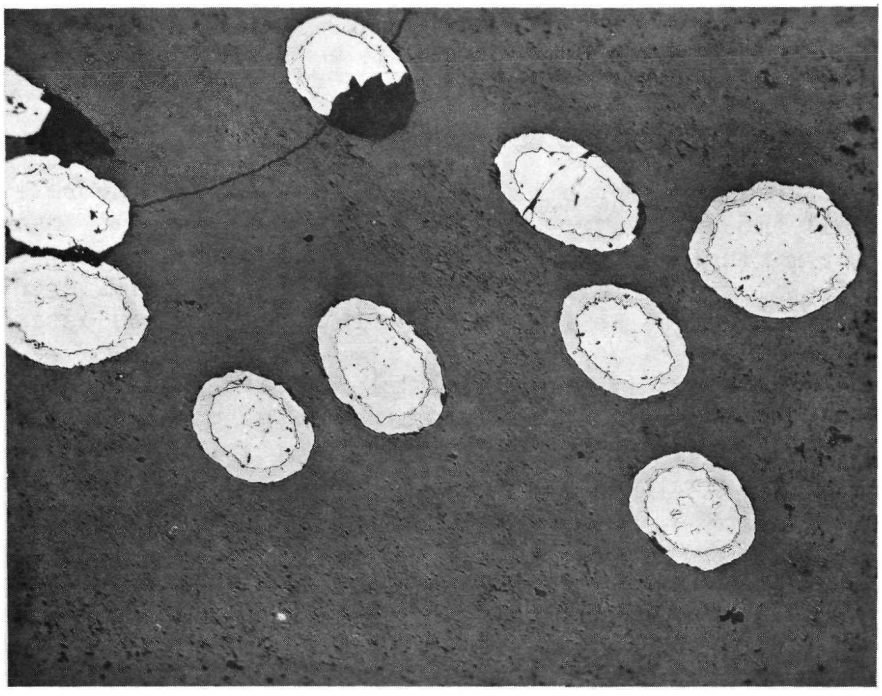

5627-1 (a) 100X

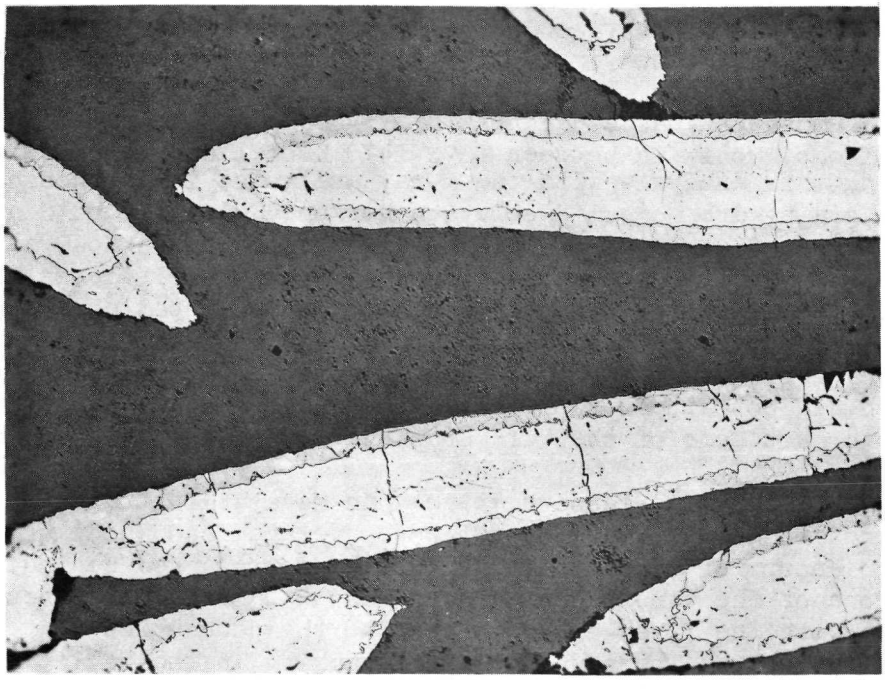

5627-2 (b) 100X

Figure 18. Etched Structure of Si_3N_4 Plus 5 v/o Mo Showing (a) Plane Parallel, and (b) Plane Perpendicular to Pressing Direction.

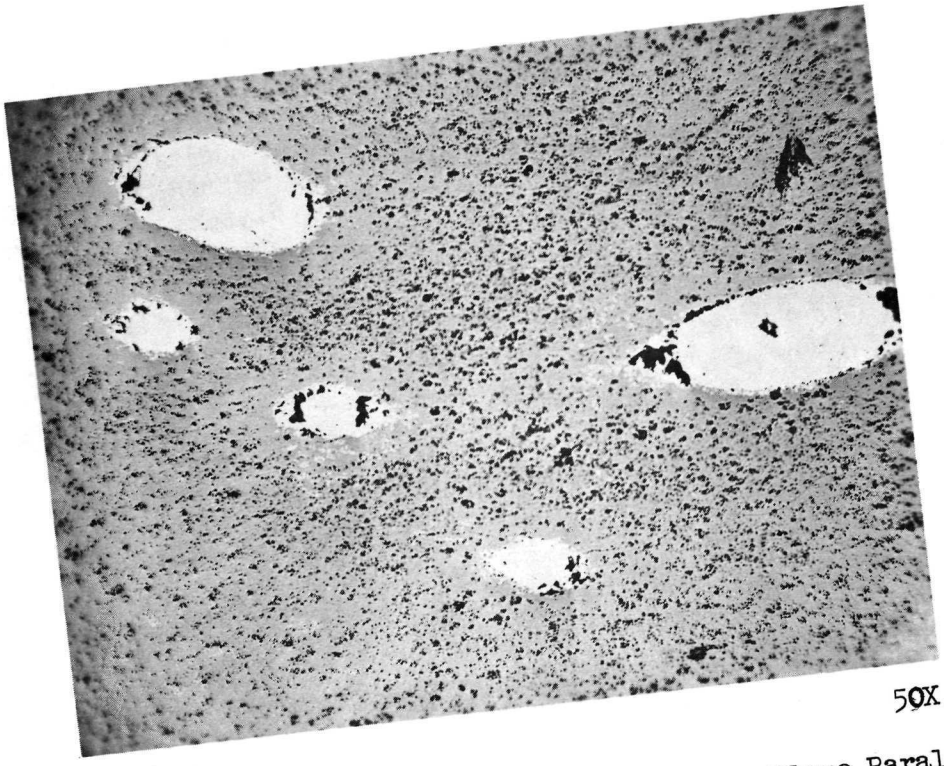

50X

5606-1

Figure 19. Si_3N_4 + 1.7 v/o Re, D1743, Illustrating Plane Parallel to the Pressing Direction.

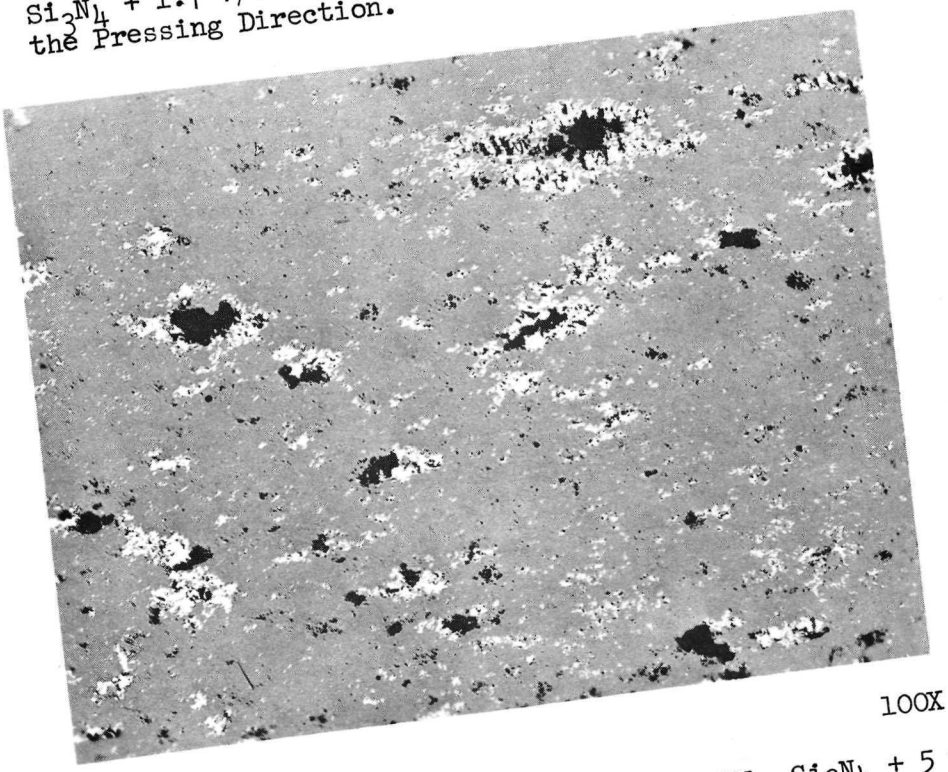

100X

5583-2

Figure 20. As-Polished Structure of D1721, Si_3N_4 + 5 v/o Cr.

decision to downgrade further work on this system.

Several pressings contained Ni20Cr powder additions, and Figure 21 illustrates the structure obtained for a 10 v/o addition. The metal phase was reasonably well distributed; however, finer dispersions might be desirable since the matrix grain size was about 1 μm. Chopped Ni20Cr wires were added to billet D1761 whose structure is illustrated in Figure 22. Based on the structure and X-ray analysis, it appears that the metal dispersed into and reacted with the Si_3N_4 matrix. The long voids are thought to represent original wire positions. Note the bridges of high reflectivity phase across one of these voids. A reacted metal silicide is the best identification for this phase.

D. Coating Studies

1. Lithium Aluminum Silicate

Coatings of β-spodumene composition ($LiAlSi_2O_6$) on Si_3N_4 were fabricated with the objective of reducing the role of existing surface cracks in impact or strength failures. Two methods of fabrication were employed for initial fabrication trials; vapor phase deposition and conventional glazing practice. The most satisfactory coatings were formed by the glazing technique.

After a 1832°F (1273°K) calcine, the $LiAlSi_2O_6$ composition was mixed into 600 centipoise H_2O base slip. The Si_3N_4 pieces were dip coated, dried, and fired at 2552°F (1673°K) for 2-3 hours.

The glazing and firing cycles have not been optimized as the coatings achieved were not of uniform thickness. The impact specimens coated were suitable for testing, however, and a typical section of the coating is illustrated in Figure 23. Mutual penetrations of the coating and matrix have occurred indicating a good bond. The coating was about 10 μm thick and consisted of at least two phases. One phase was amorphous with a diffuse reflection at 3.8 Å which corresponds to the strong reflection of α-$LiAlSi_4O_{10}$. The crystalline phases could not be positively identified, but may be one or more of the following: $Li_{0.6}Al_{0.6}Si_{2.4}O_6$, $LiAlSi_2O_6$, $LiAlSi_3O_8$, $LiAlSiO_4$, or β quartz.

2. Mechanical Polishing

Si_3N_4 impact samples were given a good metallographic polish to reduce flaw damage from grinding. Both the tension and compression sides of impact bars were polished. A tallysurf measurement of the surface roughness gave a centerline average deviation of 1.05 microinches (267 Å). The normal surface finish for both SiC and Si_3N_4 impact bars was achieved by making the final grinding passes with a 400 grit wheel. This resulted in a 11 microinch (2800 Å) centerline average deviation on the Si_3N_4 control specimens for this experiment.

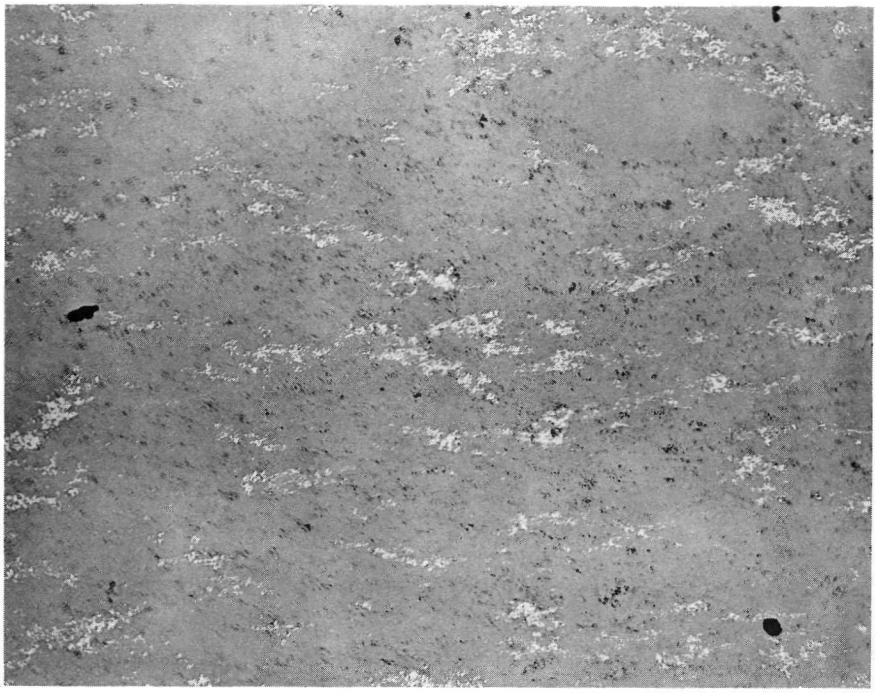

5584-4 100X

Figure 21. As-Polished Structure of D1731, Si_3N_4 Plus 10 v/o Nichrome Powder.

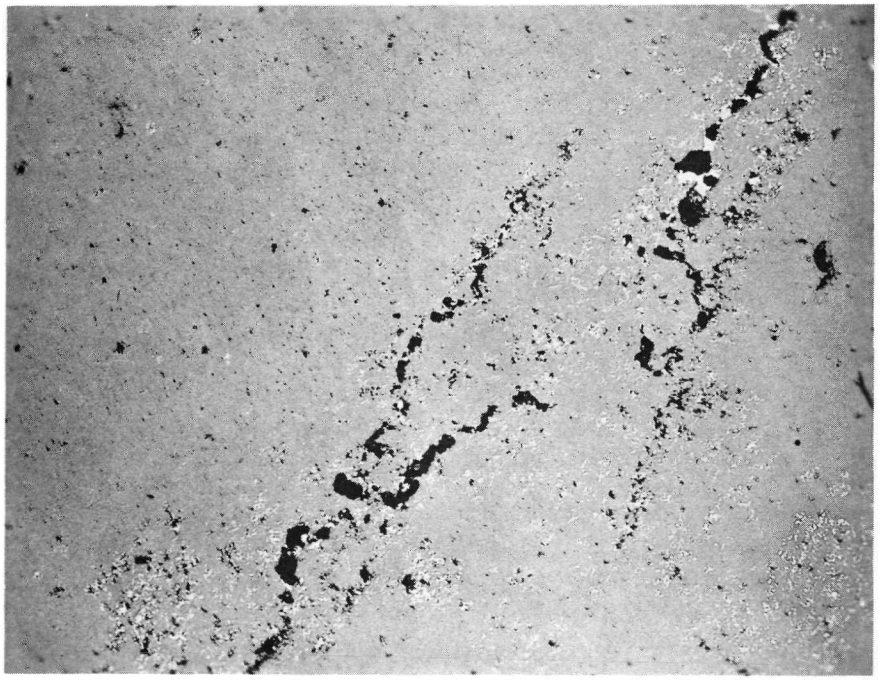

5627-3 100X

Figure 22. As-Polished Structure of Si_3N_4 Plus 10 v/o Ni20Cr Chopped Wires Illustrating Melting and Dispersion of Phase.

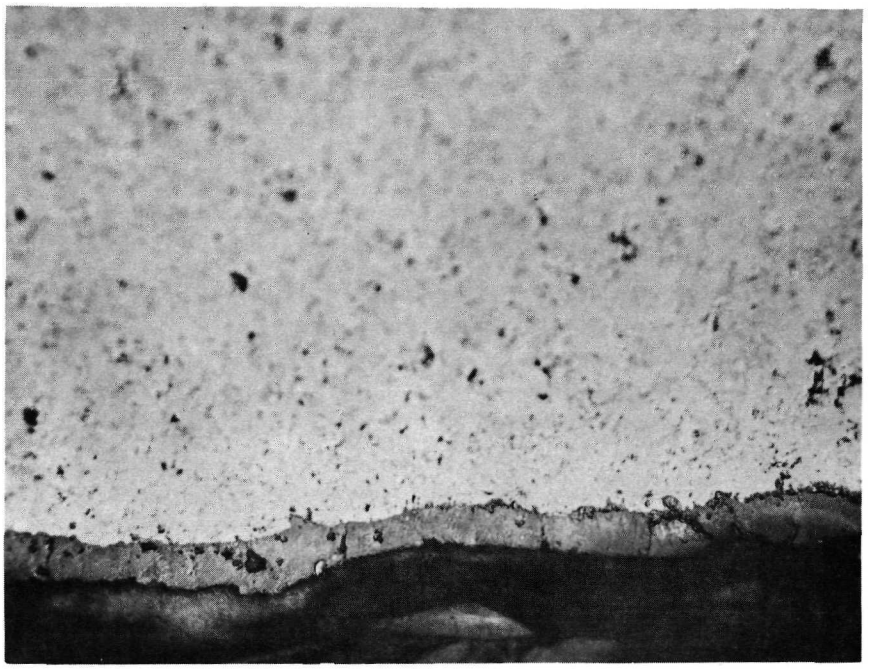

5628-2 500X

Figure 23. Cross Section of Impact Bar, 1747-6 Si_3N_4, with $LiAlSi_2O_6$ Type Coating.

IV. COMPOSITE EVALUATION

A. General

The major evaluation test was impact strength. Earlier work(ref. 1) had established that SiC and Si_3N_4 base composites possessed sufficient thermal shock resistance and thermal-chemical stability for serious consideration in the turbine application. However, the mechanical shock resistance was far lower than presently used nickel-base superalloy systems. The nickel-base superalloy B1900 had impact strengths of 108, 66, and 12 in-lbs. at 2000°F, 2100°F, and 2300°F, respectively, whereas the highest impact strength measured for a SiC or Si_3N_4 base composite in the previous program was 1.7 in-lbs. It was recognized that the impact strength measurements included the complex interaction of a number of fundamental material properties such as strength, fracture surface energy, plasticity, and rate sensitivity. Consequently, the impact strength measurement did not permit as detailed an interpretive analysis as might be desired, but it served as a very real measure of progress toward the goal of sufficient mechanical shock resistance for the turbine application. It is difficult to say precisely what value of impact strength is required for this application. A long range goal of 2-5 ft. lbs. and a short range goal of 6 ins. lbs. was established for this program.

After sufficient impact testing was accomplished to establish a promising material system, stress rupture testing was begun to determine if it had sufficient long term strength behavior to be of interest and learn if there was a correlation between this behavior, impact strength, and microstructure.

B. Mechanical Shock Resistance

A Bell Telephone Laboratories type impact tester was modified to provide impact strength data at temperatures from room to 2400°F (1589°K).(ref. 1) There is no standard test described for ceramic materials at elevated temperatures by the ASTM. However, the modified instrument does conform to the requirements of specification D256 - standard method of test for impact resistance of plastics and electrical insulating materials. The previous effort(ref. 1) provided comparison data of two superalloys; a nickel-base material - B1900, and a cobalt-base material - X40. The impact tester was modified to include some of the requirements of ASTM E23-66-Standard methods for notched bar impact testing of metallic materials. Specimens 0.250 inch (6.35×10^{-1} m) x 0.250 inch (6.35×10^{-1} m) in cross section, 2.165 inches (5.51×10^{-2} m) long with a 1.574 inch (4.00×10^{-2} m) gage length in a Charpy test mode were used. All the ceramic composite materials were tested using a 2-foot pound (2.71J) hammer while a 16-foot pound (21.7J) hammer was used for the superalloys. It was decided not to notch any specimens which constituted a departure from both ASTM D256 and ASTM E23-66. Specimens were inserted into the hot furnace and soaked for 15 minutes prior to testing.

1. SiC Base Composites

The impact strength of SiC base materials are reported in Table XIV. The data are shown graphically in Figures 24 and 25. Impact strength data for unreinforced SiC was taken from previous work.(ref. 1)

Figure 24 shows that impact strength is nearly independent of SiC whisker concentration up to 65 v/o whiskers. The 2400°F (1589°K) test at this concentration indicated some improvement. However, the fact that the 2400°F (1589°K) tests at 38 and 50 v/o were actually the lowest in their respective groups lends question to the significance of the 65 v/o - 2400°F test point. It is difficult to postulate a mechanism that would be operative at 65 v/o and not 50 v/o. The large SiC whiskers could behave as large grains giving large flaw sizes due to an increase in C of the Griffith equation (1). Thus, the fact that impact strength held relatively constant might indicate that γ_f was increased by the energy required to propagate through the high strength whiskers. The effects apparently cancel each other leaving a composite system that is not significantly improved over the matrix.

The addition of chopped C fiber as shown in Figure 25 definitely improves the impact strength of SiC. The optimum composition is between 5 and 25 v/o with 10 v/o showing one very high and one very low data point. Clearly, the composition and fabrication process require further optimization. Carbon has a high inherent γ_o; thus, the impact strength improvement is due to one of three effects: crack front interaction with the discreet fibers, high γ_o of C, high γ_f of crack extension along C/SiC interface. The fracture surfaces were considerably more irregular than unreinforced SiC, which lends support to the crack extension along the C/SiC interface mechanism. The reduction in impact strength at high volume loadings is thought to be due to the overriding effect of the large fiber size on composite strength.

TABLE XIV

Impact Test Results for SiC Base Systems

Billet	Material	Impact Strength, in.-lb. (Joules) Room Temp.	2000°F (1366°K)	2400°F (1589°K)
D1596	SiC + 38 v/o SiC	0.83 (0.094)	0.67 (0.076)	0.61 (0.069)
D1621	SiC + 50 v/o SiC	0.64 (0.072)	0.70 (0.079)	0.61 (0.069)
D1673	SiC + 65 v/o SiC	0.59 (0.067)	0.54 (0.061) *	0.96 (0.108)
D1754	SiC + 5 v/o C	0.85 (0.096)	0.96 (0.109)	1.04 (0.118)
D1745	SiC + 10 v/o C	2.09 (0.236)	0.46 (0.052)	0.88 (0.099)
D1574	SiC + 25 v/o C	1.37 (0.155)	0.96 (0.109)	0.86 (0.097)
D1594	SiC + 25 v/o C	1.16 (0.131)	1.00 (0.113)	-
D1615	SiC + 38 v/o C	0.73 (0.082)	0.64 (0.072)	0.61 (0.069)
D1679	SiC + 50 v/o C	0.84 (0.095)	0.28 (0.032) *	0.36 (0.041)

*At 2200°F, D1673 and D1679 were 0.52 and 0.39 in. lb., respectively.

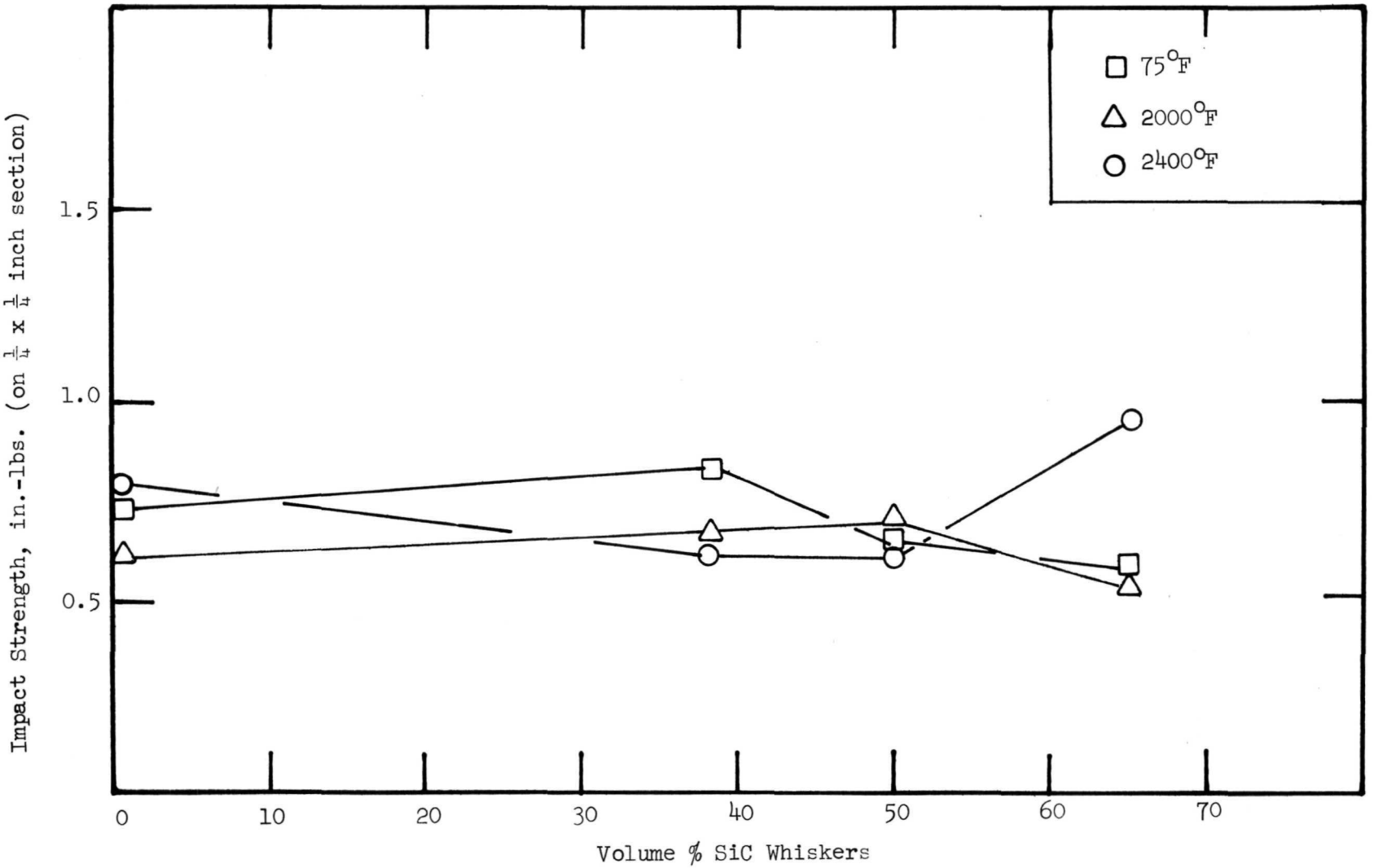

Figure 24. Impact Strength of SiC versus SiC Whisker Concentration

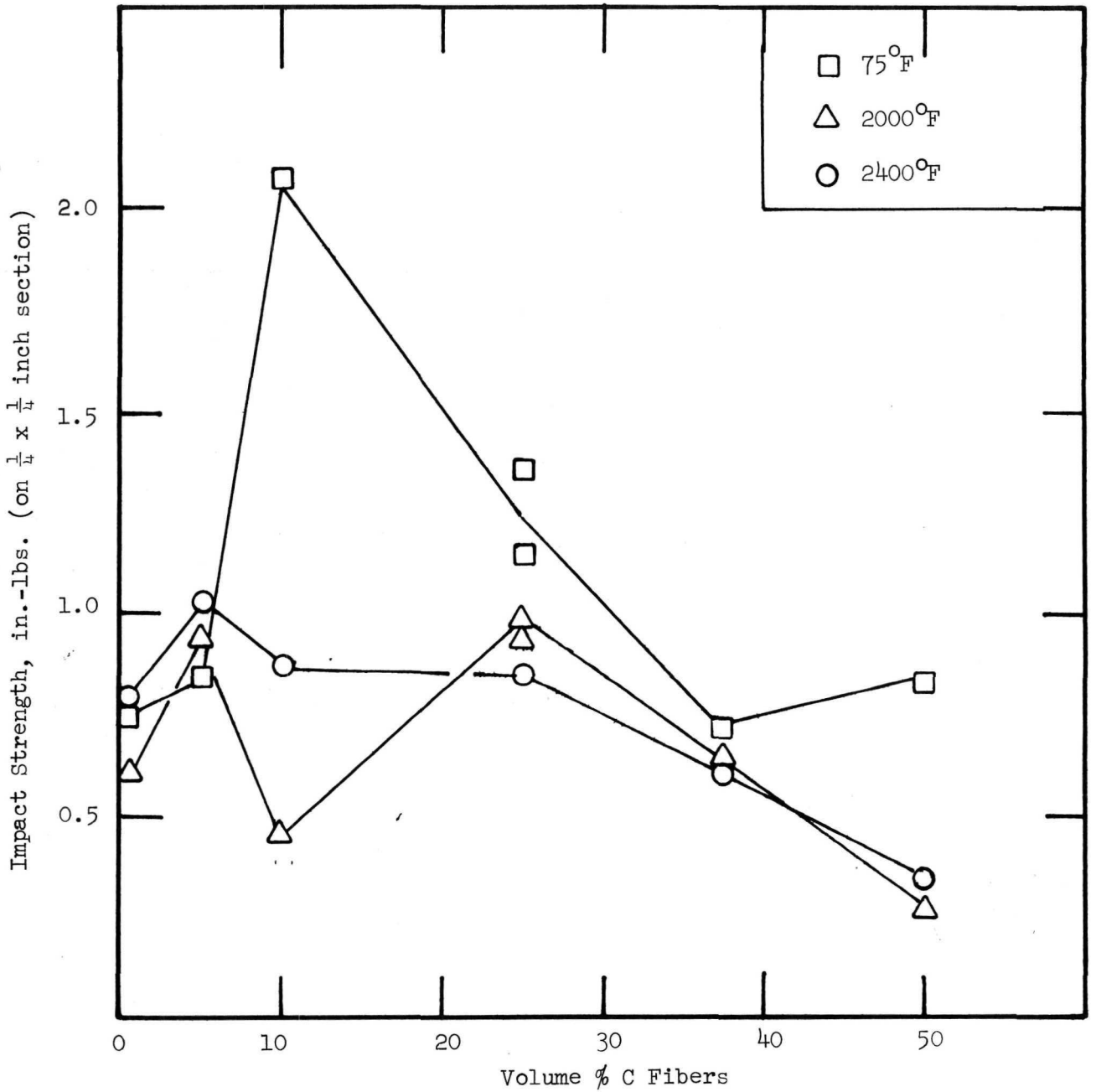

Figure 25. Impact Strength of SiC versus Carbon Fiber Concentration

2. Silicon Nitride Systems

The impact strength of Si_3N_4 base materials are reported in Table XV. Figure 26 illustrates the range of impact strengths obtained for unreinforced Si_3N_4. The strengths were a factor of 2-3 higher than those obtained on the previous program.(ref. 1) This is undoubtedly due to using high α-Si_3N_4 starting material. Lange and Terwilliger(ref. 10) argue that γ_f was the most significant factor in making high strength Si_3N_4 and that formation of an elongated microstructure was the key to obtaining high γ_f. The elongated microstructure was only achieved with α starting material. This may be an important factor, but the spread in data suggest that other factors such as phase composition, flaw density, flaw size are playing a role.

Examination of the data in Table XVI indicates that the trends predicted from a Griffith type of model approximately explain the observed effects of static and impact strength. The impact strength is increased by a factor of 1.6 to 2.6 for change from β to α starting powder. The strength increase is a factor of 1.22 to 1.62. Considering the measured impact energy to be equal to the stored elastic energy at fracture predicts that impact energy is proportional to σ_f^2; in going from β to α powder the ratio of σ_f^2 is 1.5 to 2.6, which is in the same range as impact energy increase. However, the approach is over-simplified in that it does not satisfactorily explain the differences among the various billets using α powder or the temperature dependences observed. Some of the results which SiC or β powder indicate increases in impact energy when static strength has been reduced indicating an effect of γ_f in addition to its effect on strength. Attempts to correlate the impact strength with grain size were unsuccessful. The highest, 2000°F, impact was for billets which had either retained α-Si_3N_4 or Si_2N_2O. This may be important, but the potential role of the mixed phase is uncertain. Finally, it may be mentioned that the influence of flaws on impact are thought to be determined not only by magnitude, but the duration (wavelength) of the stress pulse.(ref. 6) Thus, for impact the critical flaw may be of a different size than for static test; however, for the loading rate in a Charpy test, it is not thought this would cause a significant effect for the present materials.

The 4% MgO in D1705 does not degrade impact strength compared to the other billets containing 1% MgO. Either concentration apparently gives a continuous grain boundary phase of $MgSiO_3$ which must control high temperature properties. The upward inflection of 2400°F impact strength for D1725 must be due to increased γ_f from W_p (plastic work). Improvements in impact strength for unreinforced Si_3N_4 based on this mechanism are gained at the expense of degraded stress rupture life (Section IV.B.).

Also shown in Figure 26 are data measured on NASA supplied hot pressed Lucas Si_3N_4 which appears to be of comparable strength to the billets fabricated from AME Si_3N_4.

The data for special surface treatments to unreinforced Si_3N_4 is illustrated in Figure 27. The polished specimen gave a 10% impact strength improvement at 72°F over the control specimen. Controls were not available at other temperatures, but the 2400°F data point must reflect an impact strength improvement since it lies about 25% above the band of the Si_3N_4

TABLE XV

IMPACT TEST RESULTS FOR Si_3N_4 BASE MATERIALS

Billet	Material	Impact Strength, in. lb. (Joules) Room Temp.	2000°F (1366°K)	2400°F (1589°K)
D1562	Si_3N_4-MRC	-	-	3.30 (0.373)
D1575	Si_3N_4-MRC	2.03 (0.230)	3.88 (0.439)	3.79 (0.429)
NASA supplied Lucas	Si_3N_4 (short bar)*	3.24 (0.366) 2.95 (0.333)	2.50 (0.283)	2.03 (0.230)
D1705	Si_3N_4-AME 1	2.25 (0.254)	2.39 (0.270)	-
D1725	Si_3N_4-AME 2	2.95 (0.333)	2.36 (0.266	2.99 (0.338)
D1595	Si_3N_4-MRC (unpolished)	3.38 (0.382)	-	-
D1595	Si_3N_4 (polished)	3.52 (0.398)	2.73 (0.308)	4.94 (0.558)
D1747	Si_3N_4-AME 1 (uncoated)	2.37 (0.267)	-	-
D1747	Si_3N_4 - coated $LiAlSi_2O_6$	2.92 (0.330)	9.52 (1.075) 2.19 (0.247)	8.46 (0.956)**
D1755	Si_3N_4-AME 2	2.95 (0.333)		
D1734	Si_3N_4 + 5 v/o SiC	1.33 (0.150)	1.40 (0.158)	1.31 (0.148)
D1729	Si_3N_4 + 10 v/o SiC	1.73 (0.195)	1.46 (0.165)	0.99 (0.112)
D1752	Si_3N_4 + 10 v/o SiC (fine)	0.61 (0.069)	2.03 (0.229)	1.29 (0.146)
D1606	Si_3N_4 + 38 v/o SiC	0.83 (0.094)	0.73 (0.082)	1.85 (0.209)
D1748	Si_3N_4 + 20 v/o Si_3N_4	1.63 (0.184)	2.44 (0.276)	2.40 (0.271)
D1664	Si_3N_4 + 25 v/o Si_3N_4	0.53 (0.060)		

TABLE XV cont.

Billet	Material	Impact Strength, in. lb. (Joules) Room Temp.	2000°F (1366°K)	2400°F (1589°K)
D1610	Si_3N_4 + 25 v/o C	0.52 (0.059)	0.52 (0.059)	3.24 (0.366)
D1760	Si_3N_4 + 5 v/o Mo	0.86 (0.097)	0.86 (0.097)	0.98 (0.111)
D1743	Si_3N_4 + 1.7 v/o Re	0.88 (0.099)	0.85 (0.096)	0.93 (0.105)
D1721	Si_3N_4 + 5 v/o Cr	1.31 (0.148)	1.06 (0.120)	0.97 (0.111)
D1719	Si_3N_4 + 5 v/o Ni20Cr	2.95 (0.333)	2.05 (0.232)	1.74 (0.196)
D1731	Si_3N_4 + 10 v/o Ni20Cr	1.83 (0.207)	1.67 (0.189)	1.04 (0.117)
D1761	Si_3N_4 + 10 v/o Ni20Cr wire	1.46 (0.165)	1.27 (0.144)	1.56 (0.176)

*This bar was 0.165 inch shorter than the standard bar.
**Tested at 2300°F.

TABLE XVI

Correlation of Impact Strength and Bend Strength

Billet	Powder	Bend Strength at 2000°F	Impact Strength at 2000°F	Estimated (ref. 10) Fracture Surface Energy at 72°F	Grain Size
1251 (ref. 1)	β	41,000 psi	1.50 in.lb.	15.8×10^3 ergs/cm^2	4.7 μm
1705	α AME-1	66,500 psi	3.39 in.lb.	30×10^3 ergs/cm^2	1.7 μm
1725	α AME-2	61,700 psi	2.36 in.lb.	30×10^3 ergs/cm^2	1.0 μm
1575	α MRC	50,100 psi	3.88 in.lb.	30×10^3 ergs/cm^2	1.3 μm

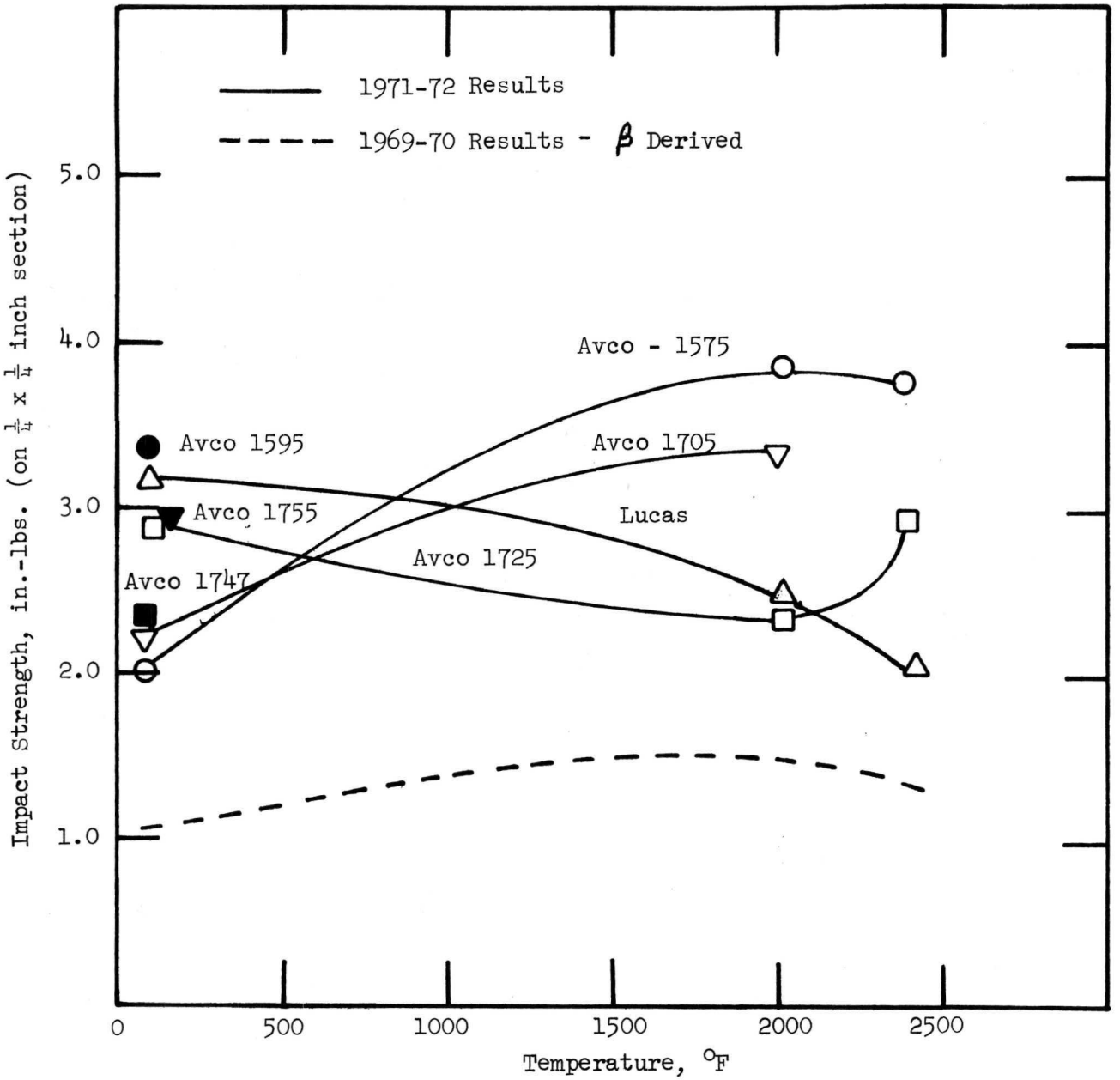

Figure 26. Impact Strength of Various Unreinforced Si_3N_4 Billets up to 2400°F

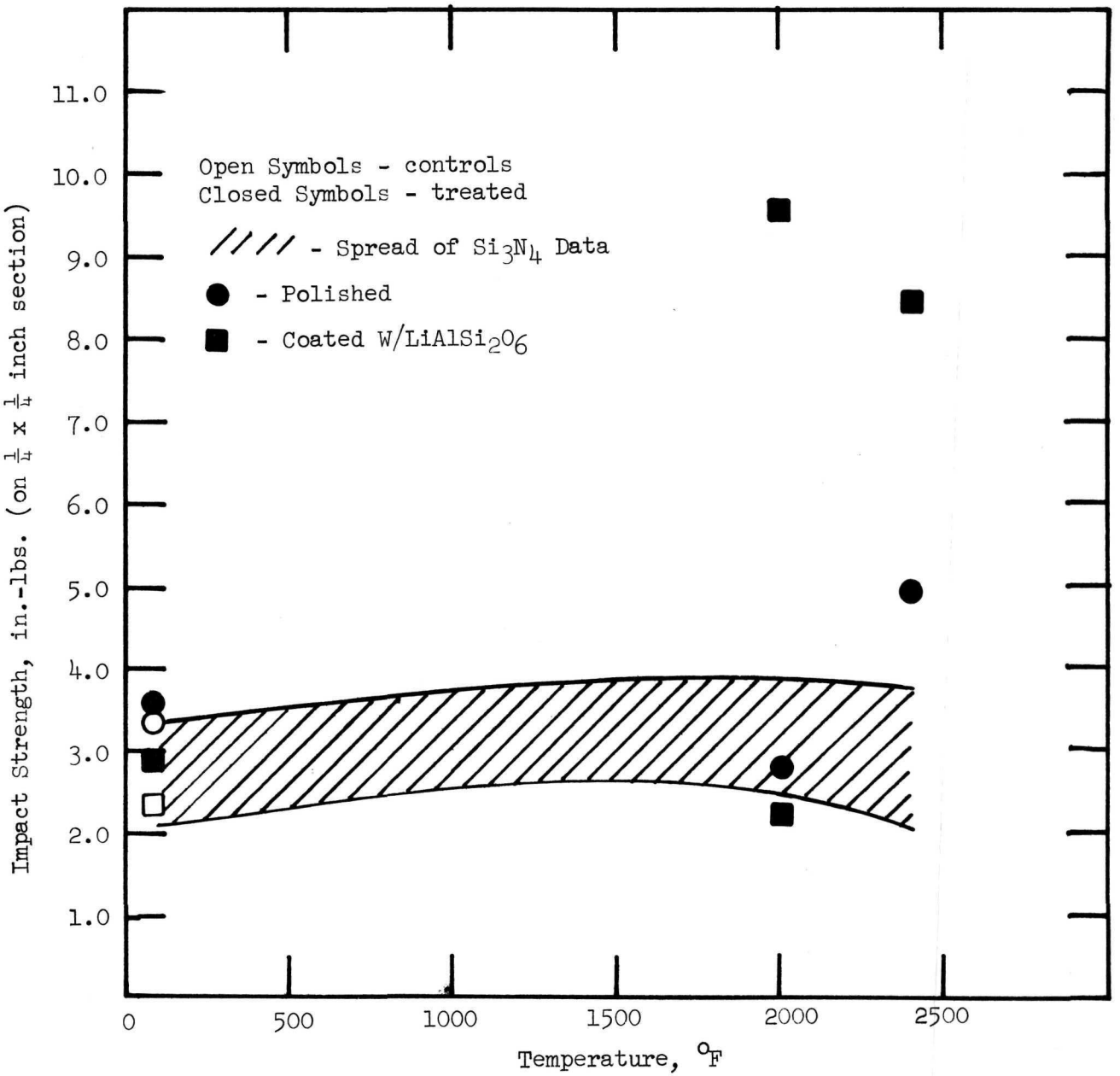

Figure 27. Effect of Surface Treatments on Si_3N_4 Impact Strength up to 2400°F

data for bars with the rougher, 11 μ inch, finish. The data indicates that microcracks created during machining are important in the failure mode during impact. This was expected at 72°F and correlates with studies on the effect of surface finish on bend strength(ref. 7). Surface flaws are predicted to be about 6 times more critical. The results indicate that stress corrosion does not dominate failure at this temperature and strain rate. (An effect of surface finish would not be observed if stress corrosion were dominant since even the polished specimens have microcracks that could be acted upon by corrosion.) The large effect at 2400°F is somewhat surprising since some plastic contribution to crack initiation and propagation was expected at 2400°F. This indicates that the strain rate was so high that the critical crack initiated motion by a brittle mechanism. Thus reducing the crack size with a finer surface finish, raised the stress level for propagation. This suggests that other effects such as thermal grooving and degree of oxidation are important variables in impact behavior. These have yet to be evaluated for Si_3N_4.

The largest improvement in impact strength was achieved by coating Si_3N_4 with a $LiAlSi_2O_6$ composition glaze. As discussed in Section III.C.1, the coating consisted of an amorphous phase and a crystalline phase that could not be positively identified. Based on visual observations, the viscosity was judged $<10^7$ poise at ≥ 2000°F. Energy absorption due to shear in the coating probably contributed to the high impact strength at elevated temperature. The nature of any other mechanisms involved is unknown. Viscous shear has a high rate sensitivity, thus there are probably other mechanisms involved in producing the high impact strength. Compressive surface layers as well as elimination of surface flaws are predicted(ref. 14) to be very important in raising impact strength. The tests were analyzed for possible interference effects and found to be completely valid tests in that regard. Clearly, this endeavor warrants more attention.

The data for Si_3N_4 plus SiC whiskers are plotted in Figure 28, and established that this approach is unpromising. The fine Carborundum whiskers gave strengths equal to the larger National Research SiC whiskers. The insensitivity to whisker size leads to the conclusion that the whiskers are not acting as flaws per se. One possible explanation is that the thermal expansion mismatch between the two components may cause microcracking leading to a large effective flaw compared with monolithic material.

Si_3N_4 plus Si_3N_4 whiskers gave moderate impact strengths. The impact strength values were higher than monolithic Si_3N_4 made from β-Si_3N_4, so the values are of interest. It is uncertain if the concept is poor or the moderate results are due to the use of impure Si_3N_4 whiskers.

The Si_3N_4/C billet tested had a poor microstructure but was tested because it was the best billet of three that were fabricated. The 72°F (295°K) and 2000°F (1366°K) tests were low, but at 2400°F (1589°K), a high impact strength value was obtained. The low impact strengths must be due to the flaws in the fabricated billets. The tests on polished Si_3N_4 specimens showed that flaws are important impact strength limiting features even at 2400°F (1589°K); thus, the high 2400°F (1589°K) test for Si_3N_4/C most probably is due to a fiber matrix interaction of the type noted for SiC/C. A second possible explanation is that the Si_3N_4 matrix has enough plasticity

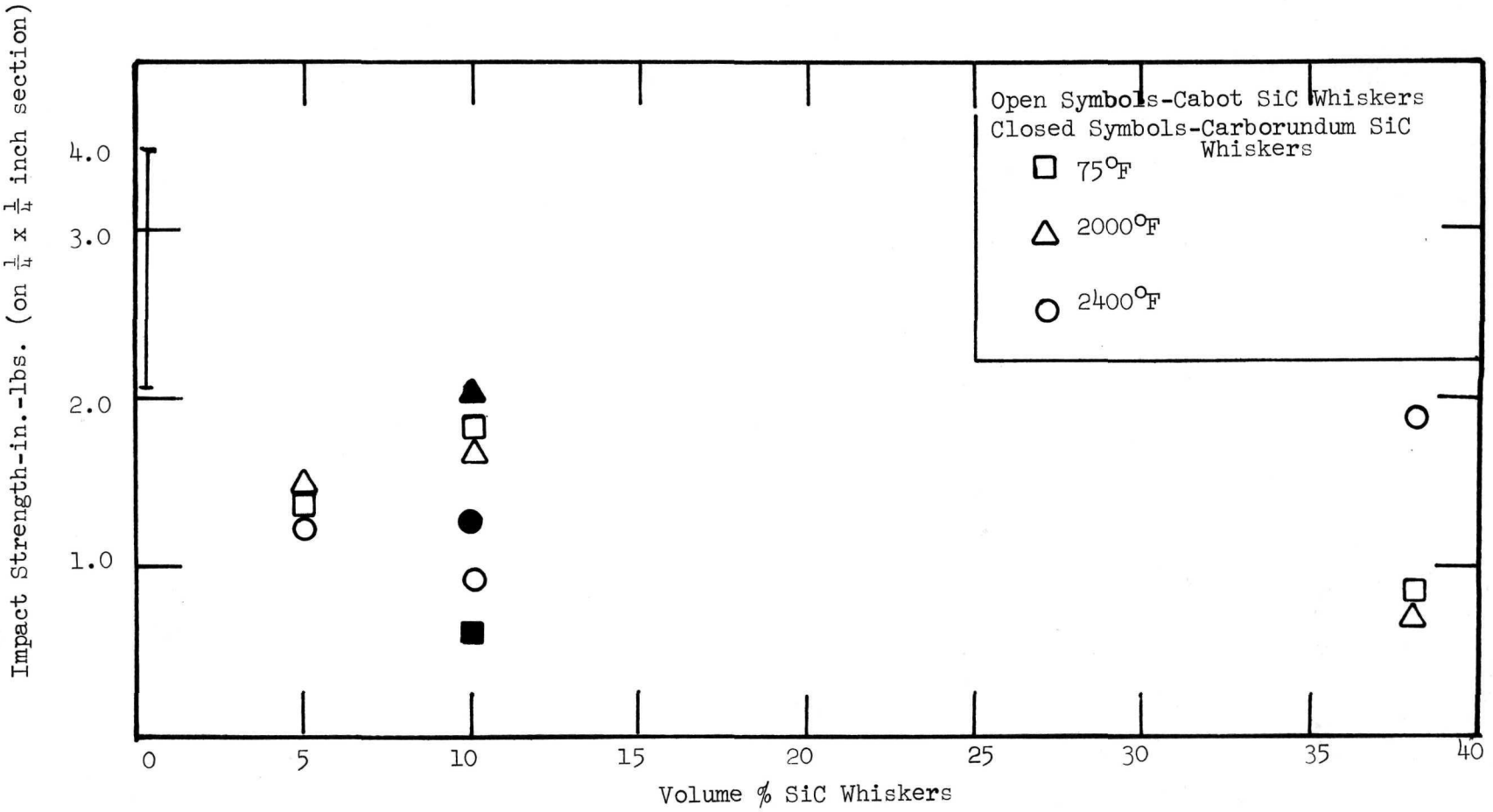

Figure 28. Impact Strength of Si_3N_4 Versus SiC Whisker Concentration

that this phase plus the $MgSiO_3$ controls the impact strength at 2400°F. There is no conclusive evidence for either mechanism. This system does hold some promise if the fabrication problems could be overcome.

The impact strength data for Si_3N_4 plus metal additions is plotted versus test temperatures in Figure 29. The impact strength for the 5 v/o Mo addition was far below the pure Si_3N_4 data at all temperatures. Mo oxidized at 2000°F (1366°K) and 2400°F (1589°K) from the outer layer leaving voids. Examination of the fracture surface established that wire was retained in the center of the impact bar. The void creation could contribute to the low impact strengths, at elevated temperatures, but the low value at 72°F is conclusive. The amount of unreacted Mo was too small to contribute markedly to increased γ_f. The long brittle mainly Mo_5Si_3 and Mo_2C phases probably increased C from the Griffith equation giving a low impact strength material.

Billet D1743, containing 1.7 v/o Re wire, was also a low impact strength billet. The Re wire morphology remained intact during testing. The oxide film over the areas where Re or ReSi intersected the surface was discolored. The impact strength results do not appear encouraging, but further work is warranted since the volume loading was so low and the reactivity with Si_3N_4 is the lowest of all the metals tested.

Of the three billets containing Cr or Ni20Cr powders, Billet D1719, containing 5 v/o Ni20Cr had the highest impact strength. In fact, the 72°F impact strength was in the high range of the pure Si_3N_4 values. The elevated temperature tests fall below the range of Si_3N_4 data which indicates that instead of aiding the impact strength, the Ni20Cr reaction phase degrades the system. The fact that a silicide forms probably results in the strength degradation. This would explain the lower impact strengths for the 10 v/o powder addition and the further degradation for the 10 v/o wire addition (D1761). The slight impact strength improvement at 2400°F (1589°K) for the latter billet is encouraging and unexplained when contrasted with the billet containing Ni20Cr powder.

C. Stress Rupture Testing

Testing was conducted in air under four-point bending mode using SiC for knife edge fixtures. The specimens were 1 3/4 x 0.100 x 0.200 inches with an outer span of 1.500 inches and an inner span of 0.500 inch. A pre-determined load was applied smoothly in a few seconds with a cam accuator on the load bearing lever arm. Strain was not measured during testing, but was calculated based on curvature on several specimens. A cut-off switch-clock circuit connected to the lever arm was utilized to detect and record failure.

Short time tests were conducted to establish base line strength values. These tests were performed in argon on specimens 0.875 x 0.050 x 0.100 inch with a 0.750 inch outer span and a 0.250 inch inner span. The induction heated unit employed HfB_2 knife edge fixtures and a constant load rate which was set to provide a nominal strain rate of about 10^{-4} sec^{-1} assuming elastic behavior.

All of the results were analyzed using the elastic beam formula:

$$\sigma = \frac{3Pa}{bh^2} \qquad (3)$$

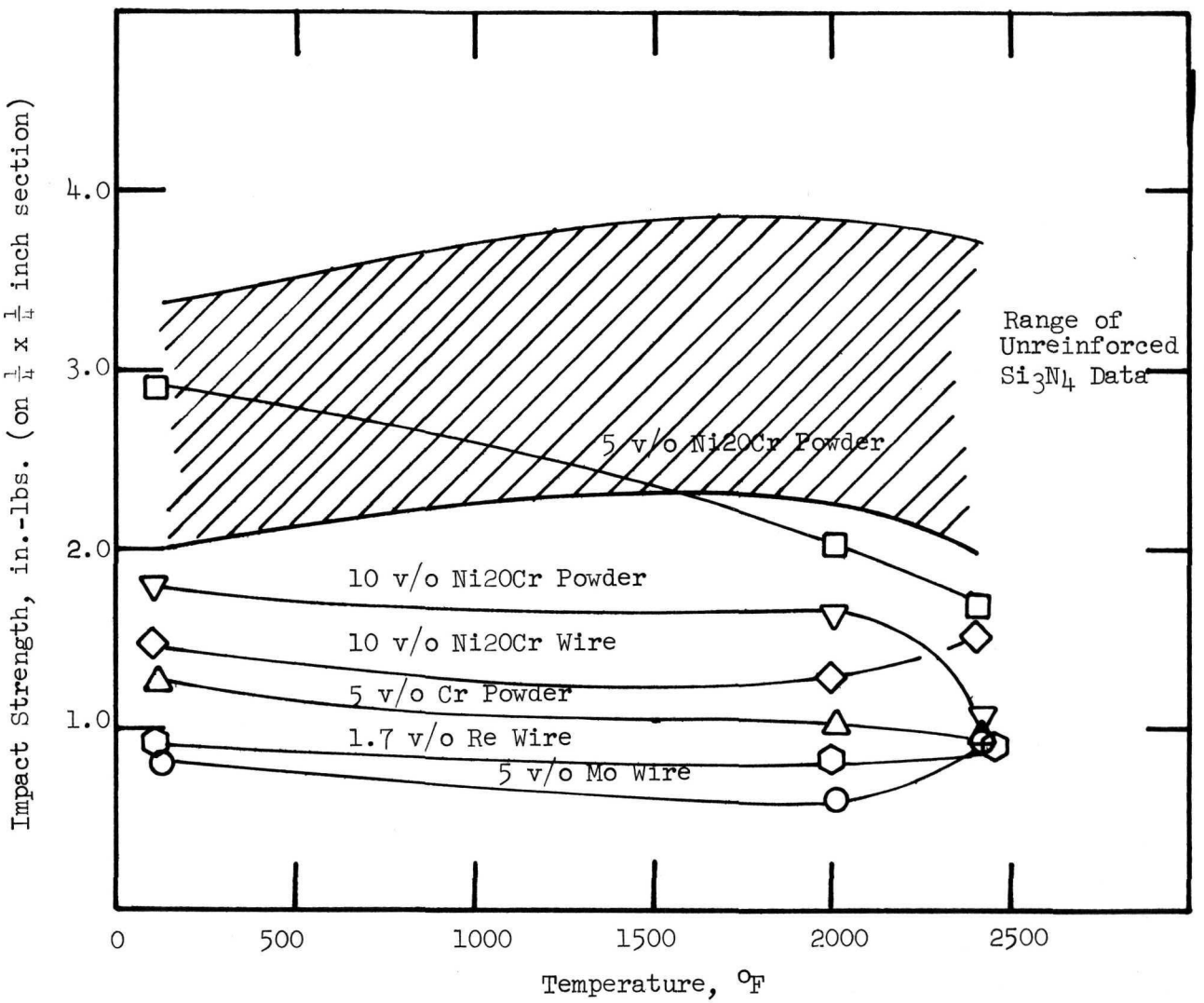

Figure 29. Effect of Various Metal Additions on Impact Strength of Silicon Nitride up to 2400°F.

where: σ = transverse rupture strength in psi

P = load, in pounds required to fracture

b = specimen width in inches

h = specimen thickness in inches

For a dead load test where plastic deformation occurs, an indication of the deviation from this formula can be obtained from the approximate equation for the steady-state stress:

$$\sigma = \frac{Pa}{bh^2} \quad (2 + m) \qquad (4)$$

where m is the strain rate sensitivity exponent. For metals, m is typically 0.2 to 0.3 so the stress will drop from its initial value to a value near that given by equation (4). For ceramics, m is typically between 0.5 and 1.0 so that there is often only a small error difference between the actual steady-state stress and the elastic stress.

Stress-rupture tests were conducted on three Si_3N_4 billets fabricated from the three α-Si_3N_4 powder lots described in Table VIII. The objective of these tests was to correlate the stress-rupture behavior with either powder properties, phase analysis, or other microstructural features. The data is presented in Figure 30, which includes the short term base line strength points. The stress-rupture points do not always extrapolate back through the short time tests presumably due to differences in testing in argon and air. Also, the times plotted for the short time tests are the total test time which exaggerates the time for comparison with the time under dead load in a stress-rupture test.

One specimen from Billet D1725 (AME-2) went 577 hours at 22,000 psi and 2000°F (1366°K) without fracture. Based on sample curvature, the strain at the end of this test time was estimated to be 0.41%. In contrast, the 18,000 psi, 2000°F (1366°K) D1575 (MRC)sample, which failed at 55 hours, was strained 0.80%. One 2400°F specimen was strained to the limit of the test fixture without failure. The strain was 1.3% in 24.6 hours at 9800 psi for a specimen from D1725 (AME-2).

The differences in the three Si_3N_4 billets were apparent in the 2000°F (1366°K) tests. Billet D1575 (MRC) exhibited two slopes with a downward trend at long times. This is indicative of the onset of a new and more severe failure mode. The fracture surfaces of the three specimens lying on the steeper curve all showed evidence for slow crack growth, whereas the higher stress, shorter time specimens had a fracture surface appearance similar to a 72°F brittle failure. An illustration of fracture surface appearance is shown in Figure 31. The particular sample shown was fractured in a short time bend test at 2400°F, but the three specimens tested at 2000°F (1366°K) all showed to varying degrees the characteristic rough and smooth areas illustrated. Figure 31b illustrates both zones and the transition from one to another (arrow). Note the high number of secondary crack branches in the rough area. Although it appears that the degree of trans-granular fracture is higher in the smooth area, this was not supported by a higher magnification examination. Thus it appears that the rough texture

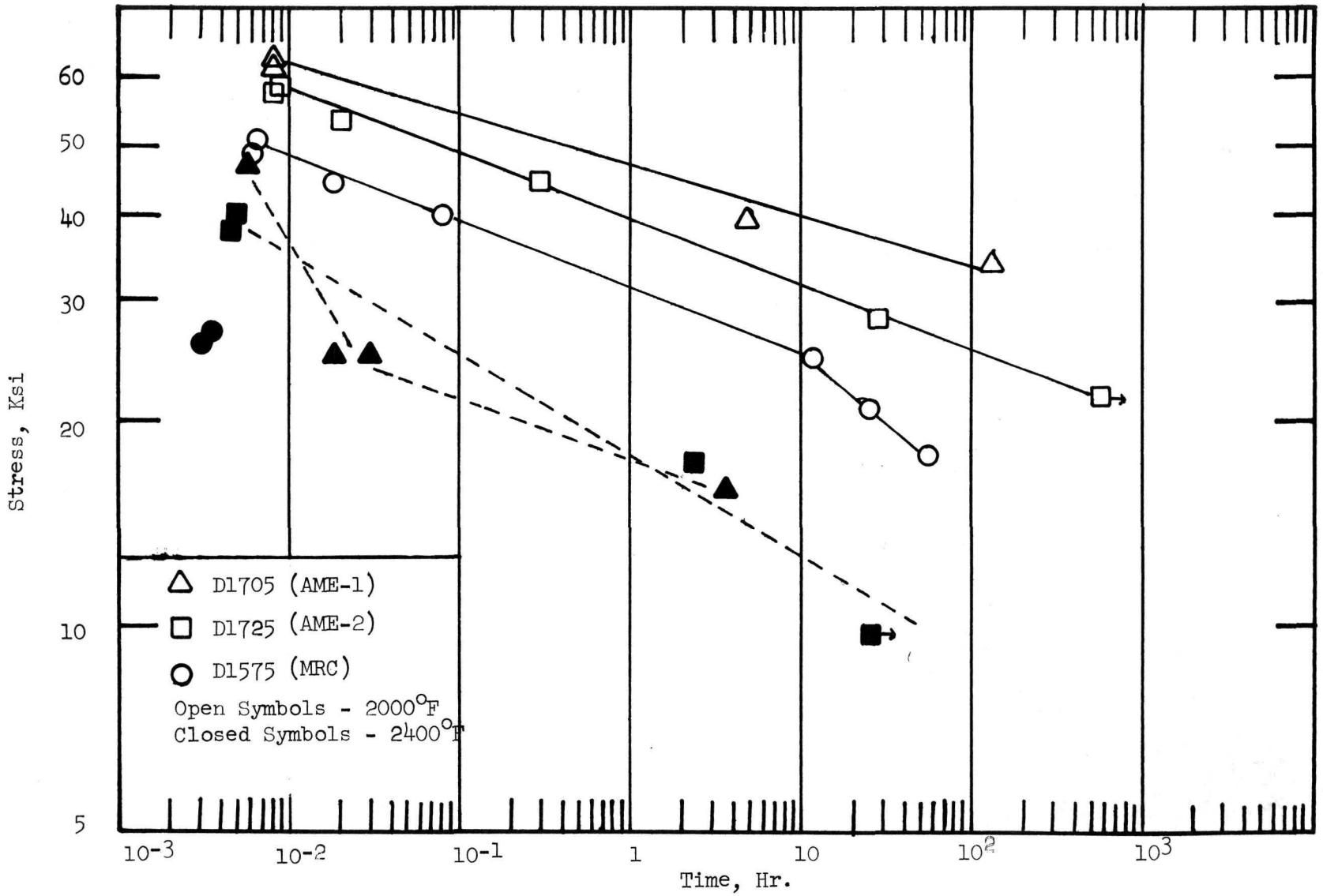

Figure 30. Stress Rupture Results for Si_3N_4

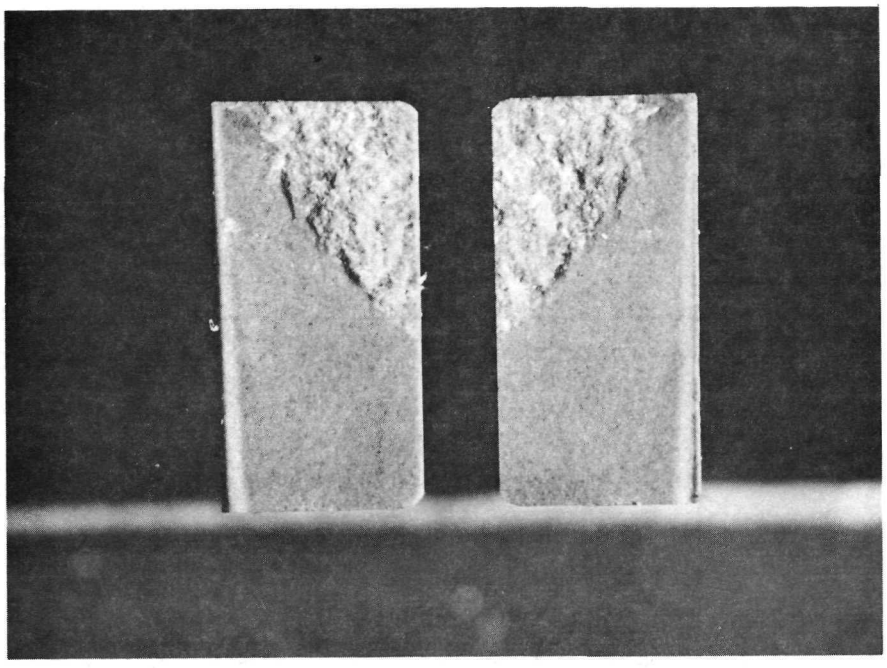

5507-2 (a) 20X

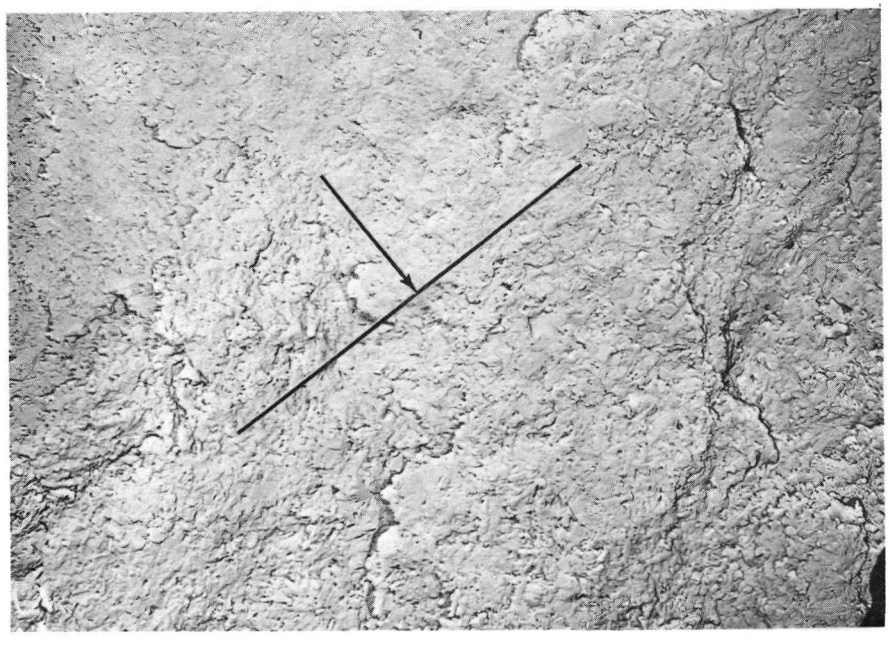

71352 (b) 1500X

Figure 31. Fracture Surfaces of Si_3N_4 - MRC (D1563) Rapid Bend Tested at 2400°F Showing (a) Matching Texture of Two Fracture Surfaces, and (b) Higher Magnification View of Rough and Smooth Structures.

is due to slow crack growth and secondary crack branching rather than a switch from intergranular to transgranular fracture. Failure occurs when these branches join and the total crack size exceeds that allowed by the Griffith criteria.

It is interesting that the short time strength values were indicative of the long term behavior. This suggests that, in a qualitative way, the same failure mechanism was operative.

The largest grain size (1.7 μm) material had the highest stress rupture strengths. This billet (D1705, AME-1) also had 4% MgO compared with 1% MgO for the other two billets. This result, along with the impact strength result, strongly suggest that the added MgO was not detrimental to strength up to 2000°F (1366°K). Even the short time, 2400°F (1589°K), strength of this billet was higher than the others; however, with the limited number of tests available, it was not possible to separate the long time behavior. The two billets tested looked approximately equal at 2400°F.

The longest test for D1705 (AME-1) at 2000°F (1366°K) also showed evidence for the slow crack growth mechanism. There was a hint of this behavior on the fracture surface for the specimen tested the next longest time. In view of the behavior for D1575 (MRC), it is surprising and unexplained why the long time D1705 (AME-1) specimens did not show the strength reduction. All of the specimens tested at 2400°F (1589°K) exhibited the fracture surfaces interpreted as due to slow crack growth.

Intermediate 2000°F (1366°K) stress-rupture strengths were obtained for D1725 (AME-2) which had a duplex grain structure, but the smallest average grain size (1.0 μm) of the billets tested. It is thought to be noteworthy that this billet was pure β-Si_3N_4 in contrast to either of the other two billets.

The lowest stress-rupture strength was measured for D1575 (MRC), which had an equiaxed intermediate grain size of 1.3 μm. This billet was ~7% Si_2N_2O in contrast to the other two billets which contained no Si_2N_2O (D1705 - AME-1 was about 23% α-Si_3N_4, however). Further, D1575 (MRC) had 3.5% porosity in contrast to the other two billets which contained about 1% pores. With this limited testing, it is not possible to establish with confidence whether it is the porosity, the equiaxed grain structure, or the Si_2N_2O responsible for the poor stress-rupture strength. It is interesting to note that the longest 2000°F (1366°K) test for this series, D1575 (MRC): 55 hrs., 18,000 psi, was strained about twice the amount for the 577 hrs., 22,000 psi, D1725 test. This suggests that the break in the D1575 (MRC) stress-rupture curve is strain dependent, and retention of the lower slope stress-rupture behavior is obtained by preventing deformation. Based on the fact that 23% α-Si_3N_4 is not detrimental, it is suspected that the porosity accounts for the poor strength and onset of cavitation which ultimately causes failure by slow crack growth. Microstructural texture was not a significant factor in the deformation of press forged Al_2O_3 (ref. 17). For this reason, the lack of texture in Si_3N_4 billet D1575 (MRC) was not thought to be responsible for the poor stress-rupture behavior.

To summarize these data, the 2000°F (1366°K) stress-rupture strengths are improved for: 1) increased grain size (some upper limit is expected, but is not yet known; 2) increased density; and 3) possibly with absence of Si_2N_2O or α-Si_3N_4. The level of MgO concentration from 1-4% is unimportant. The 2400°F testing did not differentiate material variables, but slow crack growth in all specimens suggested that plastic deformation occurred and was responsible for crack coalescence and ultimate specimen failure.

D. Comparison of Data with Current Metal Alloy Systems

The 100-hour rupture-stress was plotted in Figure 32 for the three unreinforced Si_3N_4 samples tested in this program and compared with literature data on three superalloys and Si_3N_4 produced in the previous program (ref. 1). The properties of the earlier Si_3N_4 billet (D1251) produced from β-Si_3N_4 powder were outlined in Table XVI. It is noteworthy that the billet was pressed with a 5 w/o MgO and 2 w/o C addition.

At 2000°F (1366°K), Si_3N_4 billet D1251 had a higher rupture strength than any of the superalloys or the Si_3N_4 billets fabricated from α-Si_3N_4 powder in this program. The cause of this is thought to be the larger grain size for D1251 (4.7 μm) compared with D1705 (1.7 μm), the next highest strength billet. Although the low temperature strength of D1251 was not determined, it probably is significantly lower than the billets fabricated from α-Si_3N_4. Thus it is expected that the optimum grain size will be a result of compromising low and high temperature properties (depending, of course, on the application and expected maximum stress and temperature).

The recent 2400°F (1589°K) test data did not extend to 100 hours. The points plotted are extrapolations and are thought to be approximately equivalent to the data for D1251. It was expected that lower MgO concentrations would improve the 2400°F (1589°K) rupture strengths, but these tests indicate that MgO concentrations between 1-4 wt. % give approximately equivalent strengths. Apparently, when the $MgSiO_3$ grain boundary phase is established, it dominates the 2400°F (1589°K) deformation characteristics. There may be some lower MgO concentration where the contribution of this grain boundary phase is not dominant.

V. CONCLUSIONS

The major findings of this program are listed below:

1. SiC based composites having 38-50 v/o aligned SiC whiskers were densified to high relative density. High densities were not obtained for whisker concentrations on either side of this range.

2. SiC base composites incorporating 5-38 v/o chopped, aligned C fibers densified readily; however, higher fiber loadings were only about 90% dense.

3. The Si_3N_4 microstructure was a strong function of the starting powder analysis, the concentration of additive and process thermal cycle.

4. Si_3N_4 base composites having 5-38 v/o aligned SiC whiskers densified readily while 50 v/o loading could only be densified to 90%.

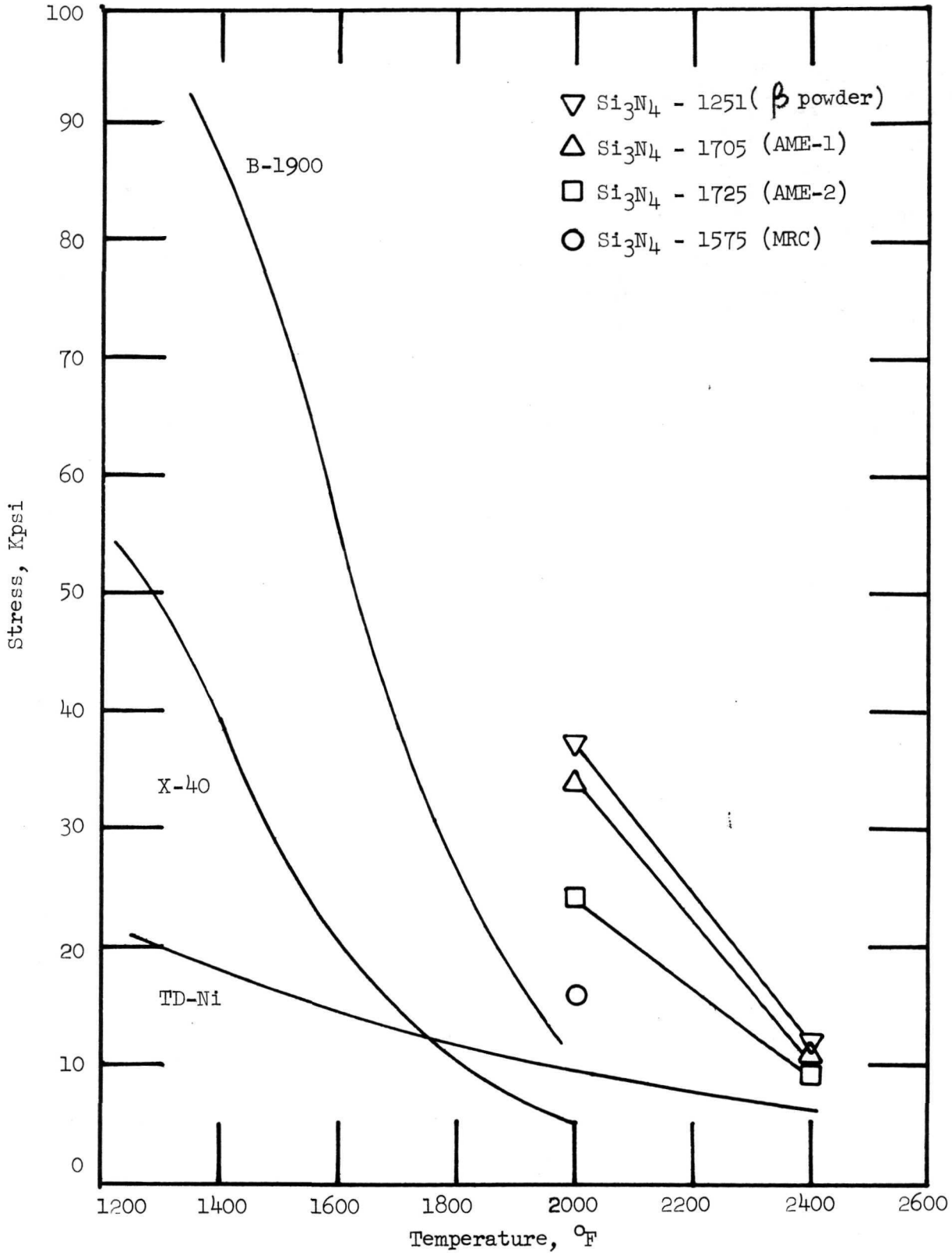

Figure 32. 100 Hour Rupture Stress Versus Temperature for Si_3N_4 Compound with Metal Alloy Systems.

5. Si_3N_4 fibers were not pure, but an acceptable microstructure of 20 v/o loading in a Si_3N_4 matrix was achieved. Both SiO_2 and C fibers reacted with Si_3N_4 during fabrication.

6. Of the metal additions to Si_3N_4, Re was the least reactive, followed by Mo. Promising composite structures were fabricated for these systems. Cr and Ni20Cr melted and reacted to form silicides.

7. Improved SiC impact strength over base line values were obtained for composites fabricated with between 5-25 v/o chopped C fibers.

8. Impact strength of Si_3N_4 was improved by up to a factor of three by coating unreinforced Si_3N_4 with $LiAlSi_2O_6$. These specimens had the highest impact strength achieved on the program and exceeded the 6 in.-lb. short range goal by 3 in.-lbs.

9. Although several of the Si_3N_4 base composites showed promising trends of impact strength, none exceeded those obtained for high density Si_3N_4 made from α-Si_3N_4 powder.

10. The 2000°F (1366°K) stress-rupture strength of Si_3N_4 was improved for increasing grain size from 1 μm to 4.7 μm, increasing relative density, and possibly with increasing phase purity. MgO concentrations between 1-4 wt. % gave equivalent strengths at both 2000°F (1366°K) and 2400°F (1589°K).

VI. REFERENCES

1. R.M. Cannon and R.J. Hill, "High Temperature Compounds for Turbine Vanes," NASA CR-72794.

2. A.A. Griffith, Phil. Trans. Roy. Soc. (London), 221A, 163 (1920).

3. I.N. Sneddon, Proc. Roy. Soc. (London), A189, 229 (1946).

4. H.G. Tattersall and G. Tappin, J. Mat. Sci., 1, 296 (1966).

5. F.J.P. Clarke, H.G. Tattersall, and G. Tappin, Proc. Brit. Ceram. Soc., 6, 163 (1966).

6. F.F. Lange,"Theory on Dispersion Toughening of Brittle Ceramics," Contract N0014-68-C-0323.

7. D.A. Schultz and H.F. Volk, "Transition Metal Diboride Composites," AFML-TR-71-41.

8. C. Herring, J. Appl. Phys., 21, 301 (1950).

9. R.A. Alliegro, L.B. Coffin, and J.R. Tinklepaugh, J. Am. Ceram. Soc. 39, 386 (1956).

10. F.F. Lange and G.R. Terwilliger, "Fabrication and Properties of Silicon Compounds," Final Report Contract N00019-17-C-0107.

11. A.F. McLean, E.A. Fisher, and D.E. Harrison, "Brittle Materials Design, High Temperature Gas Turbine," AMMRC-CTR-72-3.

12. P. Grieveson, K.H. Jack, and S. Wild, "The Crystal Chemistry of Ceramic Phases in the Silicon-Nitrogen-Oxygen and Related Systems," Progress Report No. 5, Ministry of Defense Contract N/CP.61/9411/67/4B/MP. 387 (June 1970).

13. A.L. Cunningham and R.G. Shaver, "Synthesis of Long Stable Silicon Nitride Fibers," Abstract, Bull. Am. Ceram. Soc., 48 , 503 (1969).

14. T. Lyman, editor, Metals Handbook, American Society for Metals, Metals Park, Ohio, p. 1216-20.

15. B.W. Mott, "Micro-Indentation Hardness Testing," Butterworth Scientific Publication, London, p. 249 (1956).

16. B. Steverding and S.H. Lehnigk, Bull. Am. Ceram. Soc., 49, 1057 (1970).

17. W.H. Rhodes, D.J. Sellers, R.M. Cannon, A.H. Heuer, W.R. Mitchell, and P. Burnett, "Microstructure Studies of Polycrystalline Refractory Oxides," AVSSD-0098-68-RR, Contract N00019-67-C-0336.